



**HAL**  
open science

# A Newton algorithm for steady Johnson-Segalman viscoelastic fluids based on a new non-singular log-conformation formulation and an incompressible finite element method

Pierre Saramito

► **To cite this version:**

Pierre Saramito. A Newton algorithm for steady Johnson-Segalman viscoelastic fluids based on a new non-singular log-conformation formulation and an incompressible finite element method. 2014. hal-00957244v1

**HAL Id: hal-00957244**

**<https://hal.science/hal-00957244v1>**

Preprint submitted on 9 Mar 2014 (v1), last revised 14 May 2014 (v2)

**HAL** is a multi-disciplinary open access archive for the deposit and dissemination of scientific research documents, whether they are published or not. The documents may come from teaching and research institutions in France or abroad, or from public or private research centers.

L'archive ouverte pluridisciplinaire **HAL**, est destinée au dépôt et à la diffusion de documents scientifiques de niveau recherche, publiés ou non, émanant des établissements d'enseignement et de recherche français ou étrangers, des laboratoires publics ou privés.

# A Newton algorithm for steady Johnson-Segalman viscoelastic fluids based on a new non-singular log-conformation formulation and an incompressible finite element method

Pierre Saramito

CNRS and Lab. J. Kuntzmann, B.P. 53, 38041 Grenoble cedex 9, France

**Abstract** – A new log-conformation formulation of viscoelastic fluid flows is presented in this paper. It is non-singular for vanishing Weissenberg numbers and allows a direct steady numerical resolution by a Newton method. Moreover, an exact computation of all the terms of the linearized problem is provided. The use an exact divergence free finite element method for velocity-pressure approximation and a discontinuous Galerkin upwinding treatment for stresses leads to a robust discretization. A demonstration is provided by the computation of steady solutions at high Weissenberg numbers for the difficult benchmark of the lid driven cavity flow. Numerical results are in good agreement, both qualitatively with experiment measurements on real viscoelastic flows, and quantitatively with computations performed by others authors. The numerical algorithm is both robust and very efficient, as it requires few and mesh-invariant number of linear systems resolution to reach solutions at high Weissenberg number. An adaptive mesh procedure is also presented: it permits to catch accurately both boundary layers and main and secondary vortex.

**Keywords** – Johnson-Segalman viscoelastic fluid ; matrix logarithm ; Newton method ; incompressible finite elements ; adaptive mesh ; lid-driven cavity

## Introduction

The Johnson-Segalman [32] model is considered here, i.e. the upper convective derivative in the Oldroyd-B [45] model is replaced by a mixed Gordon-Schowalter [23] derivative with a parameter  $a \in [-1, 1]$ :

$$\frac{\mathcal{D}_a \boldsymbol{\tau}}{\mathcal{D}t} = \frac{\partial \boldsymbol{\tau}}{\partial t} + (\mathbf{u} \cdot \nabla) \boldsymbol{\tau} - \boldsymbol{\tau} \mathbf{g}_a(\mathbf{u})^T - \mathbf{g}_a(\mathbf{u}) \boldsymbol{\tau}, \quad (1)$$

for all symmetric tensor  $\boldsymbol{\tau}$ , where  $\mathbf{u}$  is the velocity field and

$$\mathbf{g}_a(\mathbf{u}) = \frac{1+a}{2} \nabla \mathbf{u} - \frac{1-a}{2} \nabla \mathbf{u}^T \quad (2)$$

denotes a generalized gradient, with the convention  $\nabla \mathbf{u} = \left( \frac{\partial u_i}{\partial x_j} \right)_{1 \leq i, j \leq d}$  and  $d = 2, 3$ . Here,  $a \in [-1, 1]$  denotes the parameter of the tensor derivative. Remark that  $\mathbf{g}_a(\mathbf{u}) = W(\mathbf{u}) + aD(\mathbf{u})$  where  $D(\mathbf{u}) = (\nabla \mathbf{u} + \nabla \mathbf{u}^T)/2$  and  $W(\mathbf{u}) = (\nabla \mathbf{u} - \nabla \mathbf{u}^T)/2$  are the symmetric and skew-symmetric parts of the velocity gradient, respectively. When  $a = 1$ , then  $\mathbf{g}_1(\mathbf{u}) = \nabla \mathbf{u}$  and the Gordon-Schowalter derivative coincides with the usual upper-convected tensor derivative. When  $a = 0$ ,

we obtain the corotational derivative and when  $a = -1$ , the lower convected derivative. Problems involving such tensor derivatives appear in non-Newtonian viscoelastic polymer melt flow problems (see e.g. [55, 61]), in turbulence modeling with the  $R_{ij} - \epsilon$  Reynolds stress turbulence models, for liquid crystals [18], fiber suspension [40] or active fluids [18], where  $a$  is related to the aspect ratio of the particles in suspension. All these models introduce a relaxation time, multiplying the tensor derivative, and the corresponding dimensionless quantity is called the Weissenberg number.

The numerical computation of viscoelastic flows in non-trivial geometries has been founded from years as a very challenging enterprise. The failure of numerical methods when the Weissenberg number becomes large is known as the *high Weissenberg number problem*. In 1986, Keunings [34] observed that the maximal Weissenberg number reached by all algorithms was mesh-dependent: he deduced that this failure was due to a wrong numerical methodology. In 1987, Marchal and Crochet [43] presented numerical computations for high Weissenberg numbers with an improved numerical approach: they pointed out the need of mixed finite element methods and an upwinding treatment of the stress transport terms. This was the starting point of many numerical computations of viscoelastic flows for higher Weissenberg numbers (see e.g. [20, 56] and [47] for a review of this period). In 2000, in a review paper, Keunings [34] observed the progresses done, but pointed out that the maximal Weissenberg number reached by most reported simulations was still clearly decreasing with mesh refinement. He also concluded on the crucial role of benchmark flow problems for future works.

In 2004, Fattal and Kupferman [15, 16] remarked that some numerical instability are caused by the failure of polynomial function to approximate accurately the exponential growth of the stress tensor, due due to the presence of the deformation as a source term in the tensor transport equation. The deformation source term takes its origin in the two last terms on the right-hand side of the tensor derivative (1). The remedy proposed by these authors was a change of unknown that scale logarithmically with the stress tensor. Exploiting the fact that the conformation tensor is symmetric positive definite, the stress transport equation was reformulated as equations for the matrix logarithm of the conformation tensor (the so-called *log-conformation formulation*). Numerical experiments for the driven cavity benchmark showed that maximal Weissenberg number reached was no more mesh-sensitive [16]. This idea was a new starting point and many improved numerical computations of viscoelastic flows was then performed (see e.g. [26, 13, 1] and [10] for a recent book).

The main objective of the present paper is to bring some novelties in the challenging field of numerical methods for viscoelastic fluid flows. These novelties develops in threes main axes:

1. A new and different log-conformation formulation of viscoelastic models is proposed. This formulation is *non-singular* when the Weissenberg number vanishes, while the original one, as proposed by Fattal and Kupferman [15, 16], degenerates, due to the apparition of the inverse of the Weissenberg number in the set of equation. With the present formulation, the problem reduces nicely to the Navier-Stokes equations at zero Weissenberg number. This is a major advantage, as it opens the door of continuation methods, starting smoothly at zero Weissenberg number and increasing progressively.
2. The *steady* problem is directly solved by a Newton method, while, to our knowledge, all previous approaches with the log-conformation formulation was time-dependent (see e.g. [13]). The derivation of a robust Newton solver for the strongly nonlinear steady log-formulation is based on an *exact* computation of all the derivatives. Notice that previous Newton methods relies on some finite difference methods for computing the Jacobian matrix, as the strong non-linearities was considered as non-differentiable [33, 13].
3. The discretization bases on an *incompressible* finite element method: the discrete velocity field satisfies exactly the divergence free relation. This is a major advantage when dealing with a transport equation: Recall that a non-divergence free velocity field  $\mathbf{u}$  introduces an additional source term  $\text{div } \mathbf{u}$  in the stress transport equation: this term could then generate

an exponential growth of the stresses, and then destroy all the profit of the log-conformation formulation.

The outline of the paper is as follows. Section 1 starts with a presentation of the Johnson-Segalman model and its reformulation with the conformation tensor. Then the new non-singular log-conformation formulation is presented. The first section closes with the variational formulation of the steady problem. Section 2 begins with the space discretization by an incompressible finite element method. Then, the upwinding discretization of the transport term, based on the discontinuous Galerkin method is presented. Next, the Newton method on the discrete problem is introduced, with a special care for the derivation of highly nonlinear terms produced by the log-conformation formulation. This section closes with the Euler-Newton continuation algorithm. Section 3 presents numerical computations on the bi-dimensional driven cavity flow. A specific adaptive mesh procedure allows to catch accurately both boundary layers and secondary vortex. Finally, two appendices groups the computation of some strongly nonlinear terms and their derivatives.

## 1 Continuous setting

### 1.1 Conformation tensor formulation

Let  $\Omega \subset \mathbb{R}^d$  be a bounded open domain,  $d = 2, 3$ , and  $t_f > 0$  a final time. The Jonson-Segalman problem writes :

( $P_1$ ): find  $\tau$ ,  $\mathbf{u}$  and  $p$ , defined in  $]0, t_f[ \times \Omega$ , such that

$$\begin{aligned} \lambda \frac{\mathcal{D}_a \tau}{\mathcal{D}t} + \tau - 2\eta_p D(\mathbf{u}) &= 0 \text{ in } ]0, t_f[ \times \Omega \\ \rho \frac{D\mathbf{u}}{Dt} - \operatorname{div}(\tau + 2\eta_v D(\mathbf{u}) - p.I) &= 0 \text{ in } ]0, t_f[ \times \Omega \\ \operatorname{div} \mathbf{u} &= 0 \text{ in } ]0, t_f[ \times \Omega \\ \lambda(\tau - \tau_\Gamma) &= 0 \text{ on } ]0, t_f[ \times \partial\Omega_- \\ \mathbf{u} &= \mathbf{u}_\Gamma \text{ on } ]0, t_f[ \times \partial\Omega \\ \lambda\tau(0) = \lambda\tau_0 \text{ and } \mathbf{u}(0) &= \mathbf{u}_0 \text{ in } \Omega \end{aligned}$$

where  $\frac{D}{Dt} = \frac{\partial}{\partial t} + \mathbf{u} \cdot \nabla \mathbf{u}$  denotes the Lagrange derivative,  $\lambda \geq 0$  is the relaxation time,  $\eta_p > 0$  and  $\eta_v \geq 0$  are the polymer and solvent viscosities, respectively,  $\rho \geq 0$  is the constant density,  $\tau_0$ ,  $\mathbf{u}_0$ ,  $\tau_\Gamma$  and  $\mathbf{u}_\Gamma$  are given initial and boundary conditions and  $\partial\Omega_-$  is the upstream boundary, defined by  $\partial\Omega_- = \{x \in \partial\Omega; \mathbf{u}_\Gamma \cdot \mathbf{n}(x) < 0\}$ . The total Cauchy stress tensor is  $\boldsymbol{\sigma}_{\text{tot}} = -pI + 2\eta_v D(\mathbf{u}) + \tau$ . When  $\lambda = 0$ , the problem reduces to the Navier-Stokes equations with a total viscosity  $\eta_v + \eta_p$  and  $\tau = 2\eta_p D(\mathbf{u})$ .

There are several results available concerning the existence, uniqueness and regularity of this problem. In 1985, Renardy [53] showed an existence result for the steady problem. In 1987, Guillopé and Saut [24] proved that there exists a unique strong solution local in time and that this solution is globally defined when the data are small and the fluid is not too much elastic (see also [38] for a different approach). In 1998, Fernández-Cara, Guillén and Ortega [17] extended this result to the large elasticity case and for arbitrarily large but finite final time  $t_f$ . In 2000, Lions and Masmoudi [39] obtained an enhanced result ( $t_f$  could be infinite) in the particular case of a corotational derivative ( $a = 0$ ). In 2005, Kupferman, Mangoubi, and Titi [35] obtained a more explicit condition for the global in time existence of the solution when  $\Omega = \mathbb{R}^3$ .

The solution  $(\tau, \mathbf{u}, p)$  exhibits some important properties. Hulsen [30, p. 6, eqn(30)] (see also Kwon and Leonov [36, p. 31, eqn (10)], Lee *et al.* [37, p. 383]) introduced the following definition of the

conformation tensor when both  $a$  and  $\lambda$  are non-zero:

$$\mathbf{c} = \boldsymbol{\tau} + \frac{\eta_p}{a\lambda} I$$

where  $I$  denotes the  $d \times d$  identity matrix. Notice that  $\mathbf{c}$  has the dimension of a stress and is undefined when  $\lambda = 0$  or  $a = 0$ . Also, the conformation tensor  $\mathbf{c}$  admit an explicit expression in integral form involving the unknown velocity field  $\mathbf{u}$  [37, p. 385, eqn (3.29)]. From (1) we get  $\frac{\mathcal{D}_a I}{\mathcal{D}t} = -2aD(\mathbf{u})$  and from (1) we have  $\frac{\mathcal{D}_a \boldsymbol{\tau}}{\mathcal{D}t} = \frac{\mathcal{D}_a \mathbf{c}}{\mathcal{D}t} - \frac{2\eta_p}{\lambda} D(\mathbf{u})$ . Then, the Johnson-Segalman problem becomes:

(P<sub>2</sub>): find  $\mathbf{c}$ ,  $\mathbf{u}$  and  $p$ , defined in  $]0, t_f[ \times \Omega$ , such that

$$\lambda \frac{\mathcal{D}_a \mathbf{c}}{\mathcal{D}t} + \mathbf{c} = \frac{\eta_p}{a\lambda} I \text{ in } ]0, t_f[ \times \Omega \quad (3a)$$

$$\rho \frac{D\mathbf{u}}{Dt} - \operatorname{div}(\mathbf{c} + 2\eta_v D(\mathbf{u}) - pI) = 0 \text{ in } ]0, t_f[ \times \Omega \quad (3b)$$

$$\operatorname{div} \mathbf{u} = 0 \text{ in } ]0, t_f[ \times \Omega \quad (3c)$$

$$\lambda(\mathbf{c} - \mathbf{c}_\Gamma) = 0 \text{ on } ]0, t_f[ \times \partial\Omega_- \quad (3d)$$

$$\mathbf{u} = \mathbf{u}_\Gamma \text{ on } ]0, t_f[ \times \partial\Omega \quad (3e)$$

$$\lambda \mathbf{c}(0) = \lambda \mathbf{c}_0 \text{ and } \mathbf{u}(0) = \mathbf{u}_0 \text{ in } \Omega \quad (3f)$$

In 1990, Hulsen [30] showed that, when the initial condition  $\mathbf{c}_0$  in (3f) is symmetric definite positive, and that  $\nabla \mathbf{u}$  is bounded, then  $\mathbf{c}$  remains symmetric definite positive at any time  $t > 0$ . Notice that when  $\lambda = 0$ , the problem degenerates, due to the apparition of  $a\lambda$  in the denominator in the constitutive equation (3a). In the case of the upper convected derivative ( $a = 1$ ), Fattal and Kupferman [15, 16] introduced a change of variable  $\boldsymbol{\psi} = \log\left(\frac{a\lambda}{\eta_p} \mathbf{c}\right)$ , the so-called log-conformation formulation. Nevertheless, when  $\lambda = 0$ , the expected solution is simply  $\boldsymbol{\psi} = 0$ , while the reformulated problem still degenerates, due to a division by  $\lambda$  in the conservation of momentum equation (see [15, p. 283], the last eqn of the page). This change of variable was then applied in [11] to a generalized constitutive model that covers the present Johnson-Segalman model ( $a \in [-1, 1]$ ), but the obtained problem still degenerates when  $\lambda = 0$ . The next paragraph proposes a slightly different change of variable that solves nicely this degeneracy: the new formulation will be no more singular when  $\lambda = 0$  and this opens the possibility of building a robust steady solver based on the Newton method and a continuation algorithm, starting smoothly at  $\lambda = 0$ .

## 1.2 A new log-conformation formulation

In order to obtain a non-singular formulation, a different change of the logarithmic variable is introduced:

$$\boldsymbol{\chi} = \frac{\eta_p}{a\lambda} \log\left(\frac{a\lambda}{\eta_p} \mathbf{c}\right) = \frac{\eta_p}{a\lambda} \log\left(I + \frac{a\lambda}{\eta_p} \boldsymbol{\tau}\right) \quad (4a)$$

$$\iff \mathbf{c} = \frac{\eta_p}{a\lambda} \exp\left(\frac{a\lambda}{\eta_p} \boldsymbol{\chi}\right) \text{ and } \boldsymbol{\tau} = \frac{\eta_p}{a\lambda} \left(\exp\left(\frac{a\lambda}{\eta_p} \boldsymbol{\chi}\right) - I\right) \quad (4b)$$

Notice that both  $\boldsymbol{\chi}$ ,  $\mathbf{c}$  and  $\boldsymbol{\tau}$  have the dimension of stress. At the limit case  $a\lambda = 0$ , the new variable  $\boldsymbol{\chi}$  is still well defined, as showed by a simple Taylor expansion of the matrix logarithm at the vicinity of  $a\lambda = 0$ :

$$\boldsymbol{\chi} = \boldsymbol{\tau} - \left(\frac{a\lambda}{\eta_p}\right) \boldsymbol{\tau}^2 + \dots + \frac{1}{n} \left(\frac{a\lambda}{\eta_p}\right)^{n-1} \boldsymbol{\tau}^n + \dots$$

For instance, when  $\lambda = 0$ , then  $\boldsymbol{\tau} = 2\eta_p D(\mathbf{u})$  is the solution for the Johnson-Segalman model that reduces to a Newtonian fluid, and then  $\boldsymbol{\chi} = \boldsymbol{\tau} = 2\eta_p D(\mathbf{u})$ . For completeness, the derivation of the

present log-conformation formulation is provided here, since there is some subtle modifications due to the different change of variable and the introduction of the the Gordon-Schowalter derivative parameter  $a$ . The impatient reader can jump directly to the new formulation (8a)-(8f).

The main technique of the present derivation of the log-conformation is related to the evolution of the principal axes of the conformation tensor [31]. Recall that the symmetric positive definite matrix  $\mathbf{c}$  can always be diagonalized as  $\mathbf{c} = \mathbf{q}\tilde{\mathbf{c}}\mathbf{q}^T$  where  $\tilde{\mathbf{c}}$  is diagonal and  $\mathbf{q}$  is an orthogonal tensor, i.e.  $\mathbf{q}\mathbf{q}^T = \mathbf{q}^T\mathbf{q} = I$ . For convenience, let us denote by  $\dot{\boldsymbol{\tau}} = \frac{D\boldsymbol{\tau}}{Dt} = \frac{\partial\boldsymbol{\tau}}{\partial t} + \mathbf{u}\cdot\nabla\boldsymbol{\tau}$  the Lagrangian derivative of any tensor  $\boldsymbol{\tau}$ . Then  $\dot{\mathbf{c}} = \mathbf{q}\dot{\tilde{\mathbf{c}}}\mathbf{q}^T + \mathbf{q}\tilde{\mathbf{c}}\dot{\mathbf{q}}^T + \dot{\mathbf{q}}\tilde{\mathbf{c}}\mathbf{q}^T$ . Let us introduce  $\mathbf{r} = \mathbf{q}\dot{\mathbf{q}}^T$ . By differentiating  $\mathbf{q}\mathbf{q}^T = I$  we get  $\dot{\mathbf{q}}\mathbf{q}^T + \mathbf{q}\dot{\mathbf{q}}^T = 0$  that writes also  $\mathbf{r}^T = -\mathbf{r}$ . Then  $\mathbf{r}$  is skew-symmetric. We also obtain  $\dot{\mathbf{q}} = -\mathbf{r}\mathbf{q}$  and  $\dot{\mathbf{q}}^T = -\mathbf{q}^T\mathbf{r}^T = \mathbf{q}^T\mathbf{r}$  and then  $\dot{\mathbf{c}} = \mathbf{q}\dot{\tilde{\mathbf{c}}}\mathbf{q}^T - \mathbf{q}\tilde{\mathbf{c}}\mathbf{q}^T\mathbf{r}^T - \mathbf{r}\mathbf{q}\tilde{\mathbf{c}}\mathbf{q}^T$ . Next, let  $\tilde{\mathbf{r}} = \mathbf{q}^T\mathbf{r}\mathbf{q}$ . Remark that  $\tilde{\mathbf{r}}$  is also skew-symmetric. We have  $\mathbf{r} = \mathbf{q}\tilde{\mathbf{r}}\mathbf{q}^T$  and then

$$\dot{\mathbf{c}} = \mathbf{q} \left( \dot{\tilde{\mathbf{c}}} - \tilde{\mathbf{c}}\tilde{\mathbf{r}}^T - \tilde{\mathbf{r}}\tilde{\mathbf{c}} \right) \mathbf{q}^T \quad (5a)$$

The generalized gradient introduced in (2) decomposes in this eigensystem as  $\mathbf{g}_a(\mathbf{u}) = \mathbf{q}\tilde{\mathbf{g}}_a\mathbf{q}^T$  where  $\tilde{\mathbf{g}}_a$  is not *a priori* diagonal, since  $\mathbf{c}$  and  $\mathbf{g}_a(\mathbf{u})$  are not expected in general to share the same eigenvectors. Then  $-\mathbf{c}\mathbf{g}_a(\mathbf{u})^T - \mathbf{g}_a(\mathbf{u})\mathbf{c} = \mathbf{q} \left( -\tilde{\mathbf{c}}\tilde{\mathbf{g}}_a^T - \tilde{\mathbf{g}}_a\tilde{\mathbf{c}} \right) \mathbf{q}^T$  and the Gordon-Schowalter derivative (1) writes:

$$\frac{\mathcal{D}_a\mathbf{c}}{\mathcal{D}t} = \mathbf{q} \left( \dot{\tilde{\mathbf{c}}} - \tilde{\mathbf{c}}(\tilde{\mathbf{r}} + \tilde{\mathbf{g}}_a)^T - (\tilde{\mathbf{r}} + \tilde{\mathbf{g}}_a)\tilde{\mathbf{c}} \right) \mathbf{q}^T \quad (5b)$$

and the constitutive equation (3a) leads to

$$\dot{\tilde{\mathbf{c}}} = \frac{\eta_p}{a\lambda^2}I - \frac{1}{\lambda}\tilde{\mathbf{c}} + (\tilde{\mathbf{r}} + \tilde{\mathbf{g}}_a)\tilde{\mathbf{c}} + \tilde{\mathbf{c}}(\tilde{\mathbf{r}} + \tilde{\mathbf{g}}_a)^T \quad (5c)$$

This is a tensorial equation. Let  $(c_i)_{1 \leq i \leq d}$  be the eigenvalues of  $\mathbf{c}$ . Recall that  $\tilde{\mathbf{c}}$  is diagonal and that its  $i$ -th diagonal entry is  $c_i$ . Then, by taking the diagonal entries  $i = j$ ,  $1 \leq i \leq d$ , of the tensorial equation (5c), we get a differential equation for  $c_i$  :

$$\dot{c}_i = \frac{\eta_p}{a\lambda^2} - \left( \frac{1}{\lambda} - 2a\tilde{d}_{i,i} \right) c_i$$

where we have set  $\tilde{\mathbf{d}} = \mathbf{q}^T D(\mathbf{u})\mathbf{q} = (\tilde{d}_{i,j})_{1 \leq i,j \leq d}$ . The previous relation writes also

$$\dot{\tilde{\mathbf{c}}} = \frac{\eta_p}{a\lambda^2}I - \left( \frac{I}{\lambda} - 2a \text{diag}(\tilde{\mathbf{d}}) \right) \tilde{\mathbf{c}} \quad (5d)$$

Now, let us perform the change of variable (4a)-(4b): the problem will be rewritten in terms of

$$\boldsymbol{\chi} = \frac{\eta_p}{a\lambda} \log \left( \frac{a\lambda}{\eta_p} \mathbf{c} \right) = \mathbf{q} \frac{\eta_p}{a\lambda} \log \left( \frac{a\lambda}{\eta_p} \tilde{\mathbf{c}} \right) \mathbf{q}^T = \mathbf{q}\tilde{\boldsymbol{\chi}}\mathbf{q}^T$$

where  $\tilde{\boldsymbol{\chi}}$  is the diagonal tensor with diagonal entries

$$\chi_i = \frac{\eta_p}{a\lambda} \log \left( \frac{a\lambda}{\eta_p} c_i \right) \iff c_i = \frac{\eta_p}{a\lambda} \exp \left( \frac{a\lambda}{\eta_p} \chi_i \right), \quad 1 \leq i \leq d$$

Thus  $\dot{\tilde{\boldsymbol{\chi}}}_i = \frac{\eta_p}{a\lambda} \frac{\dot{c}_i}{c_i}$  and then, since  $\tilde{\mathbf{c}}$ ,  $\tilde{\boldsymbol{\chi}}$ ,  $\dot{\tilde{\mathbf{c}}}$  and  $\dot{\tilde{\boldsymbol{\chi}}}$  are all diagonal:

$$\begin{aligned} \dot{\tilde{\boldsymbol{\chi}}} &= \frac{\eta_p}{a\lambda} \dot{\tilde{\mathbf{c}}}\tilde{\mathbf{c}}^{-1} \\ &= \frac{\eta_p}{a\lambda} \left( \frac{\eta_p}{a\lambda^2}I - \left( \frac{I}{\lambda} - 2a \text{diag}(\tilde{\mathbf{d}}) \right) \tilde{\mathbf{c}} \right) \tilde{\mathbf{c}}^{-1}, \quad \text{from (5d)} \\ &= -\frac{1}{\lambda} \left\{ \frac{\eta_p}{a\lambda} \left( I - \frac{a\lambda}{\eta_p} \tilde{\mathbf{c}}^{-1} \right) \right\} + \frac{2\eta_p}{\lambda} \text{diag}(\tilde{\mathbf{d}}) \end{aligned}$$

From (4a), we have  $\mathbf{c}^{-1} = \frac{a\lambda}{\eta_p} \exp\left(-\frac{a\lambda}{\eta_p} \boldsymbol{\chi}\right)$  and then

$$\dot{\tilde{\boldsymbol{\chi}}} = -\frac{1}{\lambda} \left\{ \frac{\eta_p}{a\lambda} \left( I - \exp\left(-\frac{a\lambda}{\eta_p} \tilde{\boldsymbol{\chi}}\right) \right) \right\} + \frac{2\eta_p}{\lambda} \text{diag}(\tilde{\mathbf{d}})$$

Then, replacing in (5a) the instances of  $\mathbf{c}$  and  $\tilde{\mathbf{c}}$  by  $\boldsymbol{\chi}$  and  $\tilde{\boldsymbol{\chi}}$  respectively, the Lagrangian derivative of  $\boldsymbol{\chi}$  expresses:

$$\begin{aligned} \dot{\boldsymbol{\chi}} &= \mathbf{q} (\dot{\tilde{\boldsymbol{\chi}}} - \tilde{\boldsymbol{\chi}} \tilde{\mathbf{r}}^T - \tilde{\mathbf{r}} \tilde{\boldsymbol{\chi}}) \mathbf{q}^T \\ &= -\frac{1}{\lambda} \left\{ \frac{\eta_p}{a\lambda} \left( I - \exp\left(-\frac{a\lambda}{\eta_p} \boldsymbol{\chi}\right) \right) \right\} + \mathbf{q} \left( \frac{2\eta_p}{\lambda} \text{diag}(\tilde{\mathbf{d}}) - \tilde{\boldsymbol{\chi}} \tilde{\mathbf{r}}^T - \tilde{\mathbf{r}} \tilde{\boldsymbol{\chi}} \right) \mathbf{q}^T \end{aligned} \quad (5e)$$

This relation writes equivalently

$$\dot{\boldsymbol{\chi}} + \phi_a(\boldsymbol{\chi}, \nabla \mathbf{u}) + \frac{1}{\lambda} \left\{ \frac{\eta_p}{a\lambda} \left( I - \exp\left(-\frac{a\lambda}{\eta_p} \boldsymbol{\chi}\right) \right) \right\} = 0 \quad (5f)$$

where we have introduced the notation:

$$\begin{aligned} \phi_a(\boldsymbol{\chi}, \nabla \mathbf{u}) &= \mathbf{q} \tilde{\phi}_a \mathbf{q}^T \\ \tilde{\phi}_a &= \tilde{\boldsymbol{\chi}} \tilde{\mathbf{r}}^T + \tilde{\mathbf{r}} \tilde{\boldsymbol{\chi}} - \frac{2\eta_p}{\lambda} \text{diag}(\tilde{\mathbf{d}}) \end{aligned}$$

Notice that  $\phi_a(\boldsymbol{\chi}, \nabla \mathbf{u})$  is symmetric since  $\text{diag}(\tilde{\mathbf{d}})$  is diagonal and  $\tilde{\mathbf{r}} \tilde{\boldsymbol{\chi}} + \tilde{\boldsymbol{\chi}} \tilde{\mathbf{r}}^T$  is symmetric. Notice also that both  $\mathbf{q}$  and  $\text{diag}(\tilde{\mathbf{d}})$  are directly computable from  $\boldsymbol{\chi}$  and  $\nabla \mathbf{u}$  since  $\mathbf{q}$  is the tensor containing the eigenvectors of  $\boldsymbol{\chi}$  and  $\tilde{\mathbf{d}} = \mathbf{q}^T D(\mathbf{u}) \mathbf{q}$ . The computation of  $\tilde{\mathbf{r}} \tilde{\boldsymbol{\chi}} + \tilde{\boldsymbol{\chi}} \tilde{\mathbf{r}}^T$  is more technical. Let us compute  $\tilde{\mathbf{r}} = (\tilde{r}_{i,j})_{1 \leq i,j \leq d}$ . Since  $\tilde{\mathbf{r}}^T = -\tilde{\mathbf{r}}$  we have  $\tilde{r}_{i,i} = 0$ . By taking the off-diagonal entries  $i \neq j$ ,  $1 \leq i, j \leq d$ , in (5c), we get

$$0 = c_i (-\tilde{r}_{i,j} + \tilde{g}_{a;j,i}) + (\tilde{r}_{i,j} + \tilde{g}_{a;i,j}) c_j$$

where we have used  $\tilde{r}_{j,i} = -\tilde{r}_{i,j}$  and set  $\tilde{g}_{a;i,j} = \tilde{w}_{i,j} + a \tilde{d}_{i,j}$  and  $\tilde{\mathbf{w}} = \mathbf{q}^T W(\mathbf{u}) \mathbf{q} = (\tilde{w}_{i,j})_{1 \leq i,j \leq d}$ . When  $c_i \neq c_j$  we get by a simple development:

$$\tilde{r}_{i,j} = \frac{\tilde{g}_{a;i,j} c_j + \tilde{g}_{a;j,i} c_i}{c_i - c_j} = -\tilde{w}_{i,j} + a \left( \frac{c_i + c_j}{c_i - c_j} \right) \tilde{d}_{i,j} = -\tilde{w}_{i,j} + \frac{a \tilde{d}_{i,j}}{\tanh\left(\frac{a\lambda}{\eta_p} \left( \frac{\chi_i - \chi_j}{2} \right)\right)}$$

Notice that now  $\tilde{r}$  is directly computable from  $\boldsymbol{\chi}$  and  $\nabla \mathbf{u}$  but is still undetermined when  $\chi_i = \chi_j$  or  $a\lambda = 0$ . Next, always when  $i \neq j$  and  $c_i \neq c_j$ :

$$\tilde{\phi}_{a;i,j} = \chi_i \tilde{r}_{j,i} + \tilde{r}_{i,j} \chi_j = -(\chi_i - \chi_j) \tilde{r}_{i,j} = (\chi_i - \chi_j) \tilde{w}_{i,j} - \left( \frac{\frac{a\lambda}{\eta_p} \left( \frac{\chi_i - \chi_j}{2} \right)}{\tanh\left(\frac{a\lambda}{\eta_p} \left( \frac{\chi_i - \chi_j}{2} \right)\right)} \right) \frac{2\eta_p \tilde{d}_{i,j}}{\lambda}$$

As  $\lim_{x \rightarrow 0} \frac{x}{\tanh(x)} = 1$ , we obtain:

$$\tilde{\phi}_{a;i,j} = -\frac{2\eta_p}{\lambda} \tilde{d}_{i,j} \quad \text{when } \chi_i = \chi_j \quad \text{or } a\lambda = 0$$

Finally  $\phi_a(\boldsymbol{\chi}, \nabla \mathbf{u})$  is directly computable from  $\boldsymbol{\chi}$  and  $\nabla \mathbf{u}$ , in all cases. Notice that when all the eigenvalues of  $\boldsymbol{\chi}$  are equal, then  $\phi_a(\boldsymbol{\chi}, \nabla \mathbf{u}) = -\frac{2\eta_p}{\lambda} D(\mathbf{u})$ . Also, when  $a = 0$ , we have

$\phi_a(\boldsymbol{\chi}, \nabla \mathbf{u}) = \boldsymbol{\chi}W(\mathbf{u}) - W(\mathbf{u})\boldsymbol{\chi} - \frac{2\eta_p}{\lambda}D(\mathbf{u})$ . This suggest to introduce a nonlinear form  $\kappa(\cdot, \cdot)$  such that

$$\phi_a(\boldsymbol{\chi}, \nabla \mathbf{u}) = \boldsymbol{\chi}W(\mathbf{u}) - W(\mathbf{u})\boldsymbol{\chi} + \frac{\eta_p}{\lambda}\kappa\left(\frac{a\lambda}{\eta_p}\boldsymbol{\chi}, 2D(\mathbf{u})\right) - \frac{2\eta_p}{\lambda}D(\mathbf{u})$$

Then (5f) becomes

$$\lambda(\dot{\boldsymbol{\chi}} + \boldsymbol{\chi}W(\mathbf{u}) - W(\mathbf{u})\boldsymbol{\chi}) + \eta_p\kappa\left(\frac{a\lambda}{\eta_p}\boldsymbol{\chi}, 2D(\mathbf{u})\right) + \frac{\eta_p}{a\lambda}\left(I - \exp\left(-\frac{a\lambda}{\eta_p}\boldsymbol{\chi}\right)\right) = 2\eta_pD(\mathbf{u}) \quad (5g)$$

Let  $\mathbb{R}_s^{d \times d}$  denotes the set of  $d \times d$  symmetric real matrix. The form  $\kappa(\boldsymbol{\beta}, \boldsymbol{\gamma})$  is defined for all  $\boldsymbol{\beta}, \boldsymbol{\gamma} \in \mathbb{R}_s^{d \times d}$  by

$$\kappa(\boldsymbol{\beta}, \boldsymbol{\gamma}) = \mathbf{q}\tilde{\kappa}\mathbf{q}^T \quad (6a)$$

$$\tilde{\kappa}_{i,j} = \hat{\kappa}\left(\frac{\beta_i - \beta_j}{2}\right)\tilde{\gamma}_{i,j}, \quad 1 \leq i, j \leq d \quad (6b)$$

where  $\tilde{\boldsymbol{\beta}} = \mathbf{q}^T\boldsymbol{\beta}\mathbf{q} = \text{diag}(\beta_i)$  and  $\tilde{\boldsymbol{\gamma}} = \mathbf{q}^T\boldsymbol{\gamma}\mathbf{q}$ . Here,  $\hat{\kappa}(x)$  is defined for all  $x \in \mathbb{R}$  by

$$\hat{\kappa}(x) = \begin{cases} 0 & \text{when } x = 0 \\ 1 - \frac{x}{\tanh(x)} & \text{otherwise} \end{cases} \quad (6c)$$

For convenience, let us define, for all real  $\mu \geq 0$  and  $\boldsymbol{\chi} \in \mathbb{R}_s^{d \times d}$  the following function:

$$f(\mu, \boldsymbol{\chi}) = \begin{cases} 0 & \text{when } \mu = 0 \\ \frac{\exp(\mu\boldsymbol{\chi}) - I}{\mu} - \boldsymbol{\chi} & \text{otherwise} \end{cases} \quad (7)$$

Notice that the trace of  $\lambda f\left(\frac{a\lambda}{\eta_p}, \boldsymbol{\chi}\right)$  represents a local *free energy* stored by the micro-scale mechanical system (see e.g [5, 67, 46]). This concept was more recently used for stability estimates by Hu and Lelièvre [29, 7] and is reused later in this paper for automatic adaptive mesh purpose.

The new log-conformation formulation of the Johnson-Segalman problem writes:

(P<sub>3</sub>): find  $\boldsymbol{\chi}$ ,  $\mathbf{u}$  and  $p$ , defined in  $]0, t_f[ \times \Omega$ , such that

$$\lambda \frac{\mathcal{D}_0 \boldsymbol{\chi}}{\mathcal{D}t} + \boldsymbol{\chi} - f\left(\frac{a\lambda}{\eta_p}, -\boldsymbol{\chi}\right) + \eta_p\kappa\left(\frac{a\lambda}{\eta_p}\boldsymbol{\chi}, 2D(\mathbf{u})\right) - 2\eta_pD(\mathbf{u}) = 0 \quad \text{in } ]0, t_f[ \times \Omega \quad (8a)$$

$$\rho \frac{D\mathbf{u}}{Dt} - \text{div}\left(\boldsymbol{\chi} + f\left(\frac{a\lambda}{\eta_p}, \boldsymbol{\chi}\right) + 2\eta_vD(\mathbf{u}) - pI\right) = 0 \quad \text{in } ]0, t_f[ \times \Omega \quad (8b)$$

$$\text{div} \mathbf{u} = 0 \quad \text{in } ]0, t_f[ \times \Omega \quad (8c)$$

$$\lambda(\boldsymbol{\chi} - \boldsymbol{\chi}_\Gamma) = 0 \quad \text{on } ]0, t_f[ \times \partial\Omega_- \quad (8d)$$

$$\mathbf{u} = \mathbf{u}_\Gamma \quad \text{on } ]0, t_f[ \times \partial\Omega \quad (8e)$$

$$\lambda\boldsymbol{\chi}(0) = \lambda\boldsymbol{\chi}_0 \quad \text{and} \quad \mathbf{u}(0) = \mathbf{u}_0 \quad \text{in } \Omega \quad (8f)$$

where  $\boldsymbol{\chi}_0$ ,  $\boldsymbol{\chi}_\Gamma$ ,  $\mathbf{u}_0$  and  $\mathbf{u}_\Gamma$  are given. The functions  $f$  and  $\kappa$  are defined by (7) and (6a)-(6c), respectively. The elastic stress  $\boldsymbol{\tau}$  is explicitly computable from  $\boldsymbol{\chi}$  by  $\boldsymbol{\tau} = \boldsymbol{\chi} + f\left(\frac{a\lambda}{\eta_p}, \boldsymbol{\chi}\right)$  and the total Cauchy stress tensor is  $\boldsymbol{\sigma}_{\text{tot}} = -pI + 2\eta_vD(\mathbf{u}) + \boldsymbol{\tau}$ .

**REMARK 1** (Limit  $\lambda = 0$ : Newtonian fluid)  
When  $\lambda = 0$ , the problem reduces, as expected, to the Navier-Stokes equations with a total viscosity  $\eta_v + \eta_p$  and  $\boldsymbol{\chi} = 2\eta_pD(\mathbf{u})$ .



**REMARK 2** (Limit  $a = 0$ : corotational Johnson-Segalman fluid)  
When  $a = 0$ , the present log-formulation of the problem nicely reduces to the corotational Johnson-Segalman problem with  $\boldsymbol{\tau} = \boldsymbol{\chi}$  is the elastic stress, since  $f(0, \cdot)$  and  $\kappa(0, \cdot)$  both are zero, as showed in the two forthcoming properties.

**REMARK 3** (Corotational versus Gordon-Schowalter tensor derivatives)  
Notice the corotational derivative for  $\boldsymbol{\chi}$  in (8a). Thus, the present log-conformation formulation of the general Johnson-Segalman model interprets as a nonlinear perturbation with nonlinear terms ( $f$  and  $\kappa$ ) of the corotational Johnson-Segalman model. In the following section, we show that numerical treatment of corotational derivative is much more simpler than the Gordon-Schowalter one.

**PROPERTY 1** (Regularity of  $f$ )  
The function  $f$  defined by (7) is continuously differentiable and

$$f(0, \boldsymbol{\chi}) = f(\mu, 0) = 0, \quad \forall \mu \in \mathbb{R}^+, \quad \forall \boldsymbol{\chi} \in \mathbb{R}_s^{d \times d}$$

*Proof:* This result follows from a simple Taylor expansion:

$$f(\mu, \boldsymbol{\chi}) = \mu \boldsymbol{\chi}^2 \left( \frac{I}{2} + \frac{\mu \boldsymbol{\chi}}{6} + \dots + \frac{(\mu \boldsymbol{\chi})^n}{(n+2)!} + \dots + \right)$$

□

**PROPERTY 2** (Skew symmetry of  $\kappa$ )  
The function  $\kappa$  defined by (6a)-(6c) satisfies the following properties:

1.  $\kappa(\cdot, \cdot)$  is nonlinear with respect to the first variable  $\boldsymbol{\beta}$  and is linear with respect to its second variable  $\boldsymbol{\gamma}$ .
2.  $\kappa$  is traceless:

$$\text{tr } \kappa(\boldsymbol{\beta}, \boldsymbol{\gamma}) = 0, \quad \forall \boldsymbol{\beta}, \boldsymbol{\gamma} \in \mathbb{R}_s^{d \times d}$$

3.  $\kappa(\boldsymbol{\beta}, \boldsymbol{\gamma}) = 0$  when  $\boldsymbol{\beta}$  and  $\boldsymbol{\gamma}$  are aligned, i.e. share the same eigensystem. As a special case,  $\kappa(\boldsymbol{\beta}, \boldsymbol{\gamma}) = 0$  when all eigenvalues of  $\boldsymbol{\beta}$  are equal.

4.  $\kappa$  is skew-symmetric with respect to its first variable:

$$\kappa(\boldsymbol{\beta}, \boldsymbol{\gamma}) : \boldsymbol{\beta} = 0, \quad \forall \boldsymbol{\beta}, \boldsymbol{\gamma} \in \mathbb{R}_s^{d \times d}$$

The skew symmetry extends to

$$\kappa(\boldsymbol{\beta}, \boldsymbol{\gamma}) : \boldsymbol{\sigma} = 0, \quad \forall \boldsymbol{\beta}, \boldsymbol{\gamma}, \boldsymbol{\sigma} \in \mathbb{R}_s^{d \times d} \text{ and } \boldsymbol{\beta} \text{ and } \boldsymbol{\sigma} \text{ share the same eigensystem} \quad (9)$$

5.  $\kappa$  is continuously differentiable everywhere and

$$\kappa(0, \boldsymbol{\gamma}) = 0 \quad \text{and} \quad \frac{\partial \kappa}{\partial \boldsymbol{\beta}}(0, \boldsymbol{\gamma}) = 0, \quad \forall \boldsymbol{\gamma} \in \mathbb{R}_s^{d \times d}$$

*Proof:* Remark that, from (6a)-(6c), we have  $\tilde{\kappa}_{k,k} = 0$  for all  $k$ ,  $1 \leq k \leq d$  which leads to the traceless property. When  $\boldsymbol{\beta}$  and  $\boldsymbol{\gamma}$  are aligned then  $\tilde{\boldsymbol{\gamma}}$  is diagonal and then  $\tilde{\kappa}_{i,j} = 0$ . The

skew-symmetry result can be showed by a development:

$$\begin{aligned}
\kappa(\boldsymbol{\beta}, \boldsymbol{\gamma}) : \boldsymbol{\beta} &= (\mathbf{q} \tilde{\kappa} \mathbf{q}^T) : (\mathbf{q} \tilde{\boldsymbol{\beta}} \mathbf{q}^T) \\
&= \sum_{i,j,k,l,m=0}^{d-1} \mathbf{q}_{i,j} \tilde{\kappa}_{j,k} \mathbf{q}_{l,k} \mathbf{q}_{i,m} \beta_m \mathbf{q}_{l,m} \\
&= \sum_{j,k,m=0}^{d-1} \delta_{j,m} \delta_{k,m} \tilde{\kappa}_{j,k} \beta_m \quad \text{since } \sum_{i=0}^{d-1} \mathbf{q}_{i,j} \mathbf{q}_{i,m} = \delta_{j,m} \quad \text{and} \quad \sum_{l=0}^{d-1} \mathbf{q}_{l,k} \mathbf{q}_{l,m} = \delta_{k,m} \\
&= \sum_{k=1}^{d-1} \tilde{\kappa}_{k,k} \beta_k \\
&= 0 \quad \text{since } \tilde{\kappa}_{k,k} = 0
\end{aligned}$$

When  $\boldsymbol{\beta} = 0$ , then all eigenvalues of  $\boldsymbol{\beta}$  are equal and then  $\kappa(0, \boldsymbol{\gamma})$  (point 3). The proof of the differentiability of  $\kappa$  is reported in appendix A.2, as it requires some technical developments.  $\square$

### 1.3 Variational formulation of the steady problem

The variational formulation of the steady version of the log-conformation formulation (8a)-(8f) of the Johnson-Segalman problem is considered here. Moreover, the inertia term  $(\mathbf{u} \cdot \nabla) \mathbf{u}$  in the conservation of momentum (8b) is neglected: this is a common assumption in such flow simulation and the main difficulty is associated to the nonlinear terms related to the elasticity  $\lambda \geq 0$ . Let us introduce three functional spaces  $T = L^2(\Omega)^{d \times d}$  for square summable symmetric tensors,  $V(\mathbf{u}_\Gamma) = \{\mathbf{v} \in H^1(\Omega)^d; \mathbf{v} = \mathbf{u}_\Gamma \text{ on } \partial\Omega\}$  for velocities with square summable gradients and that satisfies the boundary condition and  $Q = L^2_0(\Omega) = \{q \in L^2(\Omega); \int_\Omega q \, dx = 0\}$  for square summable pressures with zero average value. Next, let the following forms, defined for all  $\boldsymbol{\chi}, \boldsymbol{\xi} \in T$ ,  $\mathbf{u}, \mathbf{v} \in H^1(\Omega)^d$ ,  $p, q \in L^2(\Omega)$  by

$$\begin{aligned}
t(\mathbf{u}; \boldsymbol{\chi}, \boldsymbol{\xi}) &= \lambda \int_\Omega ((\mathbf{u} \cdot \nabla) \boldsymbol{\chi}) : \boldsymbol{\xi} \, dx + \lambda \int_{\partial\Omega} \max(0, -\mathbf{u}_\Gamma \cdot \mathbf{n}) \boldsymbol{\chi} : \boldsymbol{\xi} \, ds \\
&\quad + \lambda \int_\Omega (\boldsymbol{\chi} W(\mathbf{u}) - W(\mathbf{u}) \boldsymbol{\chi}) : \boldsymbol{\xi} \, dx + \eta_p \int_\Omega \kappa \left( \frac{a\lambda}{\eta_p} \boldsymbol{\chi}, 2D(\mathbf{u}) \right) : \boldsymbol{\xi} \, dx \quad (10a)
\end{aligned}$$

$$l(\boldsymbol{\xi}) = \lambda \int_{\partial\Omega} \max(0, -\mathbf{u}_\Gamma \cdot \mathbf{n}) \boldsymbol{\chi}_\Gamma : \boldsymbol{\xi} \, ds \quad (10b)$$

$$a_0(\boldsymbol{\chi}, \boldsymbol{\xi}) = \int_\Omega \boldsymbol{\chi} : \boldsymbol{\xi} \, dx - \int_\Omega f \left( \frac{a\lambda}{\eta_p}, -\boldsymbol{\chi} \right) : \boldsymbol{\xi} \, dx \quad (10c)$$

$$b_1(\boldsymbol{\xi}, \mathbf{u}) = -2\eta_p \int_\Omega \boldsymbol{\xi} : D(\mathbf{u}) \, dx \quad (10d)$$

$$b_2(\boldsymbol{\chi}, \mathbf{v}) = - \int_\Omega \boldsymbol{\chi} : D(\mathbf{v}) \, dx - \int_\Omega f \left( \frac{a\lambda}{\eta_p}, \boldsymbol{\chi} \right) : D(\mathbf{v}) \, dx \quad (10e)$$

$$c(\mathbf{u}, \mathbf{v}) = 2\eta_v \int_\Omega D(\mathbf{u}) : D(\mathbf{v}) \, dx \quad (10f)$$

$$d(\mathbf{u}, q) = - \int_\Omega q \operatorname{div} \mathbf{u} \, dx \quad (10g)$$

The variational formulation writes

(FV): find  $(\boldsymbol{\chi}, \mathbf{u}, p) \in T \times V(\mathbf{u}_\Gamma) \times Q$  such that

$$t(\mathbf{u}; \boldsymbol{\chi}, \boldsymbol{\xi}) + a_0(\boldsymbol{\chi}, \boldsymbol{\xi}) + b_1(\boldsymbol{\xi}, \mathbf{u}) = l(\boldsymbol{\xi}), \quad \forall \boldsymbol{\xi} \in T \quad (11a)$$

$$b_2(\boldsymbol{\chi}, \mathbf{v}) - c(\mathbf{u}, \mathbf{v}) - d(\mathbf{v}, p) = 0, \quad \forall \mathbf{v} \in V(0) \quad (11b)$$

$$-d(\mathbf{v}, p) = 0, \quad \forall q \in Q \quad (11c)$$

The following properties are fundamental for the numerical resolution and will admit a finite-dimensional counterpart in the next section.

**PROPERTY 3** (Skew-symmetry of  $t$ )  
For all  $\boldsymbol{\chi} \in T$  and  $\mathbf{u} \in V(0)$  such that  $\operatorname{div} \mathbf{u} = 0$ , we have

$$t(\mathbf{u}; \boldsymbol{\chi}, \boldsymbol{\chi}) = 0 \quad (12)$$

*Proof:* From integration by part, we have

$$\int_{\Omega} ((\mathbf{u} \cdot \nabla) \boldsymbol{\chi}) : \boldsymbol{\chi} \, dx = - \int_{\Omega} ((\mathbf{u} \cdot \nabla) \boldsymbol{\chi}) : \boldsymbol{\chi} \, dx - \int_{\Omega} |\boldsymbol{\chi}|^2 \operatorname{div} \mathbf{u} \, dx + \int_{\partial\Omega} |\boldsymbol{\chi}|^2 \mathbf{u} \cdot \mathbf{n} \, ds$$

and since  $\mathbf{u}$  is divergence free and vanishes on the boundary, the first term of the right-hand side of (10a), giving the expression of  $t(\mathbf{u}; \boldsymbol{\chi}, \boldsymbol{\chi})$ , is zero. Next, from the skew-symmetry of  $W(\mathbf{u})$  and the symmetry of  $\boldsymbol{\chi}$  we have  $(\boldsymbol{\chi} W(\mathbf{u}) - W(\mathbf{u}) \boldsymbol{\chi}) : \boldsymbol{\chi} = 0$ . From property (9) we have  $\kappa \left( \frac{a\lambda}{\eta_p} \boldsymbol{\chi}, 2D(\mathbf{u}) \right) : \boldsymbol{\chi} = 0$  and then we get (12).  $\square$

**PROPERTY 4** (Positivity of  $a_0$ )  
For all  $\boldsymbol{\chi} \in L^2(\Omega)_s^{d \times d}$ , we have

$$a_0(\boldsymbol{\chi}, \boldsymbol{\chi}) \geq 0 \quad (13)$$

*Proof:* From (10c) and the definition (7) of  $f$ , we have

$$a_0(\boldsymbol{\chi}, \boldsymbol{\chi}) = \frac{\eta_p}{a\lambda} \int_{\Omega} \left( I - \exp \left( -\frac{a\lambda}{\eta_p} \boldsymbol{\chi} \right) \right) : \boldsymbol{\chi} \, dx$$

Observe that  $\boldsymbol{\sigma} : \boldsymbol{\tau} = \operatorname{tr}(\boldsymbol{\sigma} \boldsymbol{\tau})$  for all symmetric tensors  $\boldsymbol{\sigma}$  and  $\boldsymbol{\tau}$  and then, when  $a\lambda \neq 0$ :

$$a_0(\boldsymbol{\chi}, \boldsymbol{\chi}) = \frac{\eta_p}{a\lambda} \int_{\Omega} \operatorname{tr} \left( \left( I - \exp \left( -\frac{a\lambda}{\eta_p} \boldsymbol{\chi} \right) \right) \boldsymbol{\chi} \right) \, dx$$

As  $\boldsymbol{\chi}$  and  $\exp \left( -\frac{a\lambda}{\eta_p} \boldsymbol{\chi} \right)$  share the same eigensystem, if  $\mu$  is an eigenvalue of  $\boldsymbol{\chi}$  then  $g(\mu)$  is an eigenvalue of  $\boldsymbol{\chi} - \exp \left( -\frac{a\lambda}{\eta_p} \boldsymbol{\chi} \right) \boldsymbol{\chi}$  where  $g(\mu) = \mu - \exp(-a\lambda\mu/\eta_p)\mu$ . An easy inspection of the variation of  $g$  shows that  $g(\mu) \geq 0$  for all  $\mu \in \mathbb{R}$ . Then, we obtain the result (13).  $\square$

**REMARK 4** (Corotational versus Gordon-Schowalter tensor derivatives (cont.))  
Multiplying (1) by  $\boldsymbol{\tau}$ , integrating and rearranging leads to

$$\int_{\Omega} \frac{\mathcal{D}_a \boldsymbol{\tau}}{\mathcal{D}t} : \boldsymbol{\tau} \, dx = \frac{1}{2} \frac{d}{dt} \left( \int_{\Omega} |\boldsymbol{\tau}|^2 \, dx \right) - 2a \int_{\Omega} \operatorname{tr}(\boldsymbol{\tau} D(\mathbf{u}) \boldsymbol{\tau}) \, dx$$

When  $a \neq 0$ , there is no way to determine the sign of the last term of the right-hand side of the previous relation. The corresponding term  $-a(\boldsymbol{\tau} D(\mathbf{u}) + D(\mathbf{u}) \boldsymbol{\tau})$ , ported by  $a \neq 0$  in the tensor derivative (1), acts as a source term in any tensorial transport problem involving the general Gordon-Schowalter derivative, such the initial and conformation formulations of the Johnson-Segalman problem. This term is responsible of the observed exponential growth of the stress tensor  $\boldsymbol{\tau}$  and the failure of numerical methods. There is no hope to obtain either a skew-symmetry or a positivity property for such problems, and this especially true for the popular upper-convected derivative ( $a = 1$ ). On the contrary, the log-conformation formulation involves a corotational tensor derivative of  $\boldsymbol{\chi}$  in (8a): this leads to the skew-symmetry of  $t$  and the positivity of  $a_0$ . Properties 3 and 4 are definitive advantages of the present log-conformation formulation to the initial or the conformation one.

Remark also that, when using initially a corotational derivative ( $a = 0$ ), there is no more need of the log-conformation formulation. In that case, observe that the new formulation presented here nicely reduces to the initial one with  $\boldsymbol{\chi} = \boldsymbol{\tau}$  while all the extra nonlinear terms disappear.

## 2 Discretization and numerical resolution

### 2.1 Space approximation

The main idea is to replace the three spaces  $T$ ,  $X$ ,  $Q$  by some finite dimensional counterparts  $T_h \subset T$ ,  $X_h \subset X$ ,  $Q_h \subset Q$  in the variational formulation (11a)-(11c). When  $\lambda = 0$  (i.e. a Newtonian fluid), a finite dimensional linear system is then obtained, whose matrix has the following bloc structure:

$$\begin{pmatrix} A & B^T & 0 \\ B & -C & -D^T \\ 0 & -D & 0 \end{pmatrix}$$

This linear system is often called the *three field Stokes problem* and the approximation space pairs  $(T_h, X_h)$  and  $(X_h, Q_h)$  have both to satisfy a compatibility condition, known as the inf-sup or Babuška-Brezzi condition [8, 21, 9]. There are many possible choices for  $T_h$ ,  $X_h$  and  $Q_h$  each of them having some advantages and drawbacks. In this paper, we consider the following choice (see

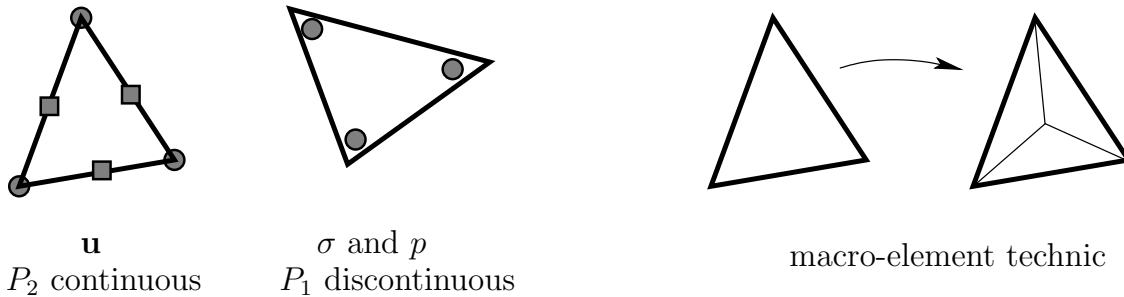


Figure 1: Incompressible element for the three-field Stokes problem.

Fig. 1):

$$\begin{aligned} T_h &= \{\tau_h \in T; \tau_{h|K} \in P_1, \forall K \in \mathcal{T}_h\} \\ X_h &= \{\mathbf{v}_h \in (H^1(\Omega) \cap C^0(\bar{\Omega}))^d; \mathbf{v}_{h|K} \in P_2, \forall K \in \mathcal{T}_h\} \\ V_h(\mathbf{g}) &= X_h \cap V(\pi_h(\mathbf{g})) \\ Q_h &= \{q_h \in Q; q_{h|K} \in P_1, \forall K \in \mathcal{T}_h\} \end{aligned}$$

where  $\mathcal{T}_h$  is a finite element mesh of the flow domain  $\Omega$  and  $h > 0$  denotes the largest edge length of the mesh. Notice that both  $T_h$  and  $Q_h$  contain *discontinuous* piecewise polynomials while  $X_h$  elements are continuous. The discontinuous approximation of stresses has two advantages. From one hand,  $D(X_h) \subset T_h$  and then the compatibility condition between  $T_h$  and  $X_h$  is satisfied for the bi-linear form  $b_1$ , as showed by Fortin and Pierre [21, 20]. From other hand, it allows an efficient treatment of the stress transport term by the discontinuous Galerkin method.

The discontinuous approximation of pressure has also a major advantage. As  $\text{div}(X_h) \subset Q_h$ , it leads to an exact *divergence free* approximation of the velocity: for any field  $\mathbf{v}_h \in X_h$  satisfying  $d(\mathbf{v}_h, q_h) = 0$  for all  $q_h \in Q_h$ , we have  $\text{div } \mathbf{v}_h = 0$  point-wise everywhere in  $\Omega$ . The pair  $(X_h, Q_h)$  is known as the Scott-Vogelius lowest-order finite element approximation [63]. This is a major advantage when dealing with a transport equation. The only drawback is that the pair  $(X_h, Q_h)$  do not satisfy the inf-sup condition for an arbitrary mesh. Nevertheless, there is a remedy: Arnold and Qin [3] proposed a macro element technique applied to the mesh [3] that permits to satisfy the inf-sup condition: for any triangular finite element mesh, it is sufficient to split each triangle in three elements from its barycenter (see Fig. 1). This technique has been implemented for the present computations. Notice that the macro element technique extends to quadrilateral meshes [3] and to the three-dimensional case [68].

Let us review and discuss some other possible choices for the discretization of the problem.

- A very popular choice is to use staggered finite difference grids for velocity and pressure the velocity-pressure pair. With this choice the approximate velocity fields are also exactly divergence free, the finite-difference implementation is simple and this element also extends nicely in the mixed finite element context with the incompressible Raviart-Thomas finite element [22, chap. 3]. For the stress approximation, there are several possibilities: in [55, p. 17], the present author used also a staggered grid approximation (diagonal stress components at cell centers and off-diagonal components at cell corners in the bi-dimensional case). With this choice, the stress-velocity pair satisfies the inf-sup condition and leads to a robust scheme that is able to reach solutions for high Weissenberg numbers (see [56, 62]). In [16, p. 27], Fattal and Kupferman used a cell centered approximation for all the stress components. As pointed out by these authors [16, p.29]:

*”This implies that the rotational components of the system may be sensitive to numerical instabilities. A natural remedy would have been to store the off-diagonal elements of the stress tensor at cell corners. This cannot be done in our framework as the log-conformation tensor is an entity whose tensorial nature is essential.”*

See also point 6 of the discussion, p. 36 of the same paper. With this choice, it is not clear whether the stress-velocity pair satisfies the inf-sup condition. Nevertheless, using this approximation, these authors was also able to compute solutions for some high Weissenberg numbers. A possible explanation of this success can be founded in a paper by Baranger and Sandri [4]: these authors have shown that the stress-velocity compatibility condition exhibited by [21] is only required when  $\eta_v/(\eta_v + \eta_p) \ll 1$ , i.e. in the absence of the pure viscous contribution. Otherwise, when  $\eta_v$  is not too small as compared with  $\eta_p$ , a much larger class of discretization schemes is allowed. This last condition was fulfilled by Fattal and Kupferman: all the computations presented by these authors used  $\eta_v = \eta_p$ .

- A classical choice is the Taylor-Hood  $P_2 - P_1$  continuous element [66] (see also [9, p. 252]) for the velocity-pressure spaces  $(X_h, Q_h)$  while stresses are piecewise linear and discontinuous. This choice for the stress approximation was first introduced by A. and M. Fortin [20]. Damanik [12, p. 25] used recently a variant for quadrilaterals meshes, combining  $Q_2$  continuous velocities with  $P_1$  discontinuous pressure [9, p. 216] and quadratic continuous approximation of stresses. As  $\text{div}(X_h) \not\subset Q_h$ , for these elements, the approximate velocity field are not exactly divergence free: this is the main difference with the Scott-Volelius used in the present computation. We performed tests for both the Taylor-Hood approximation and the  $Q_2 - P_{1,d}$  variant for quadrilaterals, together with  $P_{1,d}$  stresses, on the driven cavity problem and observed that the steady approximate solution presents some troubles: for large dimensionless Weissenberg numbers (e.g.  $We = 1$ ), the divergence  $\text{div } \mathbf{u}_h$  do no more converge to zero with mesh refinement  $h \rightarrow 0$ . It could be due to the low regularity of the velocity field in boundary layers of the cavity, especially at high Weissenberg numbers. This observation motivates the use the divergence-free approximation for the velocity-pressure pair.
- Another possible choice is to use constant and discontinuous  $P_0$  stresses while the velocity-pressure space pair  $(X_h, Q_h)$  is still the divergence free Scott-Vogelius one, as in the present paper. Notice that we have now  $D(X_h) \not\subset Th$ . This choice was first suggested by Mangoubi and Boyaval [42, 6, 7] in a theoretical paper and these authors was able to show a nice stability property for the free energy. There was no numerical experiments available to our knowledge with this combination and we also performed some test on the driven cavity problem: we observed that this choice is less robust and less precise than when choosing piecewise linear and discontinuous stresses as presented here.

This discretization review is far from complete and exhaustive: there is many other possible approaches and many of some of them has been already experimented. Nevertheless, observe

that the exact divergence free property for the approximation of the velocity field appears as an essential condition in such flow simulations. Both the staggered finite difference method and the Scott-Vogelius finite element one for the velocity-pressure pair satisfies this condition. The Scott-Vogelius finite element method presents two additional advantages as compared with the finite difference one: (i) it allows the same approximation for all the stress components while satisfying the inf-sup condition and (ii) it is more flexible when dealing with complex geometries or adaptive mesh.

## 2.2 Approximation of the transport term

Let us turn to the discretization of the nonlinear stress transport term by the discontinuous Galerkin method. We introduce the following form, defined for all  $\mathbf{u} \in H^1(\Omega)^d$  and  $\boldsymbol{\chi}, \boldsymbol{\xi} \in L^2(\Omega)_s^{d \times d}$  such that  $\boldsymbol{\chi}|_K, \boldsymbol{\xi}|_K \in H^1(K)_s^{d \times d}$  for all element  $K \in \mathcal{T}_h$ :

$$\begin{aligned} t_h(\mathbf{u}; \boldsymbol{\chi}, \boldsymbol{\xi}) &= \lambda \sum_{K \in \mathcal{T}_h} \int_K ((\mathbf{u} \cdot \nabla) \boldsymbol{\chi}) : \boldsymbol{\xi} \, dx + \lambda \sum_{S \in \mathcal{S}_h^{(i)}} \int_S \llbracket \boldsymbol{\chi} \rrbracket : \left( \frac{\theta}{2} |\mathbf{u} \cdot \mathbf{n}| \llbracket \boldsymbol{\xi} \rrbracket - (\mathbf{u} \cdot \mathbf{n}) \{ \boldsymbol{\xi} \} \right) \, ds \\ &\quad + \lambda \int_{\partial\Omega} \max(0, -\mathbf{u}_\Gamma \cdot \mathbf{n}) \boldsymbol{\chi} : \boldsymbol{\xi} \, ds + \lambda \int_{\Omega} (\boldsymbol{\chi} W(\mathbf{u}) - W(\mathbf{u}) \boldsymbol{\chi}) : \boldsymbol{\xi} \, dx \\ &\quad + \int_{\Omega} \kappa \left( \frac{a\lambda}{\eta_p} \boldsymbol{\chi}, 2D(\mathbf{u}) \right) : \boldsymbol{\xi} \, dx \end{aligned} \quad (14)$$

where  $\mathcal{S}_h^{(i)}$  denotes the set of internal sides of the mesh  $\mathcal{T}_h$  and  $\llbracket \boldsymbol{\xi} \rrbracket$  is the jump of a piecewise discontinuous tensor across a side and  $\{ \boldsymbol{\xi} \}$  is its average value [14, 60]. The three first terms represent a discrete counterpart of the transport term, that can not be defined globally since the stress approximation is piecewise discontinuous. A term is weighted by a factor  $\theta \geq 0$ : choosing  $\theta = 0$  corresponds to the so-called centered flux approximation, while  $\theta > 0$  is the *upwinding* flux approximation. The case  $\theta = 1$ , that is the most popular upwinding discontinuous approximation scheme, is considered here. The upwinding technique is known as an efficient approach to avoid spurious oscillations of the approximate solutions.

The discrete variational formulation of the problem writes:

(FV)<sub>h</sub>: find  $\boldsymbol{\chi}_h \in T_h$ ,  $\mathbf{u}_h \in V_h(\mathbf{u}_\Gamma)$  and  $p_h \in Q_h$  such that

$$\begin{aligned} t_h(\mathbf{u}_h; \boldsymbol{\chi}_h, \boldsymbol{\xi}_h) + a_0(\boldsymbol{\chi}_h, \boldsymbol{\xi}_h) + b_1(\boldsymbol{\xi}_h, \mathbf{u}_h) &= l(\boldsymbol{\xi}_h), \quad \forall \boldsymbol{\xi}_h \in T_h \\ b_2(\boldsymbol{\chi}_h, \mathbf{v}_h) - c(\mathbf{u}_h, \mathbf{v}_h) - d(\mathbf{v}_h, p_h) &= 0, \quad \forall \mathbf{v}_h \in V_h(0) \\ -d(\mathbf{u}_h, q_h) &= 0, \quad \forall q_h \in Q_h \end{aligned}$$

The continuous tri-linear form  $t$  has simply been replaced by  $t_h$  and the functional spaces by their finite dimensional counterpart.

**PROPERTY 5** (Discrete generalized skew-symmetry)  
For all  $\boldsymbol{\chi}_h \in T_h$  and  $\mathbf{u}_h \in V_h(0)$  such that  $\text{div } \mathbf{u}_h = 0$ , we have

$$t_h(\mathbf{u}_h; \boldsymbol{\chi}_h, \boldsymbol{\chi}_h) \geq 0 \quad (15)$$

with an equality when  $\theta = 0$ .

*Proof:* Integrating by part on an element  $K$  leads to

$$\int_K ((\mathbf{u}_h \cdot \nabla) \boldsymbol{\chi}_h) : \boldsymbol{\chi}_h \, dx = - \int_K \boldsymbol{\chi}_h : ((\mathbf{u}_h \cdot \nabla) \boldsymbol{\chi}_h) \, dx + \int_K |\boldsymbol{\chi}_h|^2 (\mathbf{u}_h \cdot \mathbf{n}) \, dx$$

since  $\operatorname{div} \mathbf{u}_h = 0$ . Then

$$\sum_{K \in \mathcal{T}_h} \int_K ((\mathbf{u}_h \cdot \nabla) \boldsymbol{\chi}_h) : \boldsymbol{\chi}_h \, dx = \frac{1}{2} \sum_{K \in \mathcal{T}_h} \int_{\partial K} |\boldsymbol{\chi}_h|^2 (\mathbf{u}_h \cdot \mathbf{n}) \, ds = \frac{1}{2} \sum_{S \in \mathcal{S}_h^{(i)}} \int_S [|\boldsymbol{\chi}_h|^2] (\mathbf{u}_h \cdot \mathbf{n}) \, ds$$

Remark that, for any discontinuous scalar field  $\phi$  and  $\varphi$  across a side  $S$ , we have  $[[\phi\varphi]] = [[\phi]]\{\{\varphi\}\} + \{\{\phi\}\}[[\varphi]]$ . Then  $[|\boldsymbol{\chi}_h|^2]/2 = [[\boldsymbol{\chi}_h]] : \{\{\boldsymbol{\chi}_h\}\}$  and

$$\sum_{K \in \mathcal{T}_h} \int_K ((\mathbf{u}_h \cdot \nabla) \boldsymbol{\chi}_h) : \boldsymbol{\chi}_h \, dx = \sum_{S \in \mathcal{S}_h^{(i)}} \int_S [[\boldsymbol{\chi}_h]] : \{\{\boldsymbol{\chi}_h\}\} (\mathbf{u}_h \cdot \mathbf{n}) \, ds$$

Using  $\mathbf{u}_h = 0$  on  $\partial\Omega$  and dealing with the two last terms of (14) as in the proof of property 3, we obtain:

$$t_h(\mathbf{u}_h; \boldsymbol{\chi}_h, \boldsymbol{\chi}_h) = \frac{\theta\lambda}{2} \sum_{S \in \mathcal{S}_h^{(i)}} \int_S [|\boldsymbol{\chi}_h|]^2 |\mathbf{u}_h \cdot \mathbf{n}| \, ds$$

which completes the proof. □

**PROPERTY 6** (Discrete positivity)  
For all  $\boldsymbol{\chi}_h \in T_h$ , we have

$$a_0(\boldsymbol{\chi}_h, \boldsymbol{\chi}_h) \geq 0 \tag{16}$$

*Proof:* As  $T_h \subset L^2(\Omega)_s^{d \times d}$ , this result is a direct consequence of property 4. □

### 2.3 Newton method

Newton methods for the numerical resolution of steady viscoelastic flow problem started in 1987 with the work of Marchal and Crochet [43]. In 1992, Fortin and Zine [19] proposed a quasi-Newton variant, where the Jacobian matrix was approximated instead of being completely recomputed at each iteration. After a long time, the Newton method approach for viscoelastic fluid problems comes back. While previous works relies on some finite difference methods for computing the Jacobian matrix, in 2009, Howell [28] computed exactly the linearized problem for the steady Johnson-Segalman problem in its initial formulation. In 2010, Damanik et al [13, 12] turned to a Newton method for the time-dependent log-conformation formulation. These last authors used a finite difference method for computing the Jacobian matrix. Let us quote a remark made in 2009 by Kane, Gu enette, and Fortin [33, p. 45] for the log-conformation formulation:

*"[...] there is no hope to fully linearize the constitutive equations for the Newtons method without using some numerical tricks such as finite difference methods. The bulk of the computations relies indeed on the calculation, at each Gauss node, of the eigenvalues and eigenvectors of the conformation tensor which are not differentiable functions".*

In the present paragraph, an exact expression of the derivatives for the fully linearized constitutive equation is presented for log-conformation formulation, without any trick such as finite difference methods for computing the Jacobian matrix. The present Newton method directly treats the steady problem: by an obvious extension, it applies also to fully implicit time dependent simulations.

The discrete problem can be put in a compact form:

find  $(\boldsymbol{\chi}_h, \mathbf{u}_h, p_h) \in T_h \times V_h(\mathbf{u}_\Gamma) \times Q_h$  such that

$$F(\lambda; (\boldsymbol{\chi}_h, \mathbf{u}_h, p_h)) = 0$$

where  $F$  is defined in variational form for all  $(\boldsymbol{\xi}_h, \mathbf{v}_h, q_h)$  by

$$\begin{aligned} \langle F(\lambda; (\boldsymbol{\chi}_h, \mathbf{u}_h, p_h)), (\boldsymbol{\xi}, \mathbf{v}, q) \rangle &= t_h(\mathbf{u}_h; \boldsymbol{\chi}_h, \boldsymbol{\xi}_h) + a_0(\boldsymbol{\chi}_h, \boldsymbol{\xi}_h) + b_1(\boldsymbol{\xi}_h, \mathbf{u}_h) - l(\boldsymbol{\xi}_h) \\ &\quad + b_2(\boldsymbol{\chi}_h, \mathbf{v}_h) - c(\mathbf{u}_h, \mathbf{v}_h) - d(\mathbf{v}_h, p_h) \\ &\quad - d(\mathbf{u}_h, q_h) \end{aligned}$$

and where  $\langle \cdot, \cdot \rangle$  stands for the duality product induced by the  $L^2$  pivot space, i.e.  $\langle \varphi, \phi \rangle = \int_\Omega \varphi \phi \, dx$  for all  $\varphi, \phi$  defined in  $\Omega$ . The function  $F$  has two variables  $\lambda \in \mathbb{R}^+$  and  $U = (\boldsymbol{\chi}_h, \mathbf{u}_h, p_h) \in T_h \times X_h \times Q_h$ . The  $\lambda$  variable will be used as a continuation parameter in the next section. The Newton method defines the sequence  $(\boldsymbol{\chi}_h^{(k)}, \mathbf{u}_h^{(k)}, p_h^{(k)})_{k \geq 0}$  by recurrence as:

- $k = 0$ : let  $(\boldsymbol{\chi}_h^{(0)}, \mathbf{u}_h^{(0)}, p_h^{(0)}) \in T_h \times V_h(\mathbf{u}_\Gamma) \times Q_h$  being given.
- $k \geq 0$ : let  $(\boldsymbol{\chi}_h^{(k-1)}, \mathbf{u}_h^{(k-1)}, p_h^{(k-1)}) \in T_h \times V_h(\mathbf{u}_\Gamma) \times Q_h$  being known.  
Find  $(\delta \boldsymbol{\chi}_h, \delta \mathbf{u}_h, \delta p_h) \in T_h \times V_h(0) \times Q_h$  such that

$$\frac{\partial F}{\partial U} \left( \lambda; (\boldsymbol{\chi}_h^{(k-1)}, \mathbf{u}_h^{(k-1)}, p_h^{(k-1)}) \right) \cdot (\delta \boldsymbol{\chi}_h, \delta \mathbf{u}_h, \delta p_h) = -F \left( \lambda, (\boldsymbol{\chi}_h^{(k-1)}, \mathbf{u}_h^{(k-1)}, p_h^{(k-1)}) \right)$$

and then defines

$$\boldsymbol{\chi}_h^{(k)} = \boldsymbol{\chi}_h^{(k-1)} + \delta \boldsymbol{\chi}_h, \quad \mathbf{u}_h^{(k)} = \mathbf{u}_h^{(k-1)} + \delta \mathbf{u}_h \quad \text{and} \quad p_h^{(k)} = p_h^{(k-1)} + \delta p_h$$

At each step  $k \geq 0$ , this algorithm solves a linear subproblem involving the Jacobian  $\frac{\partial F}{\partial U}$ . The Newton method has only local convergence properties, i.e. the initial data should be close enough to the solution. In order to circumvent this limitation, a globalized Newton variant is used here: it bases on a damped strategy, as described and implemented in the `Rheolef` free software FEM library [59]. Notice the absolute value function that appears in the upwinding term in the definition (14) of  $t_h$ :

$$s_h(\mathbf{u}_h; \boldsymbol{\chi}_h, \boldsymbol{\xi}_h) = \frac{1}{2} \sum_{S \in \mathcal{S}_h^{(i)}} \int_S [[\boldsymbol{\chi}_h]] : [[\boldsymbol{\xi}_h]] |\mathbf{u}_h \cdot \mathbf{n}| \, ds$$

This term is not differentiable with respect to  $\mathbf{u}_h$ , and so are  $t_h$  and  $F$ . Nevertheless, the absolute value is convex and some tools from the subdifferential calculus can be used to circumvent this new difficulty. Let us introduce the multi-valued sign function:

$$\text{sgn}(x) = \begin{cases} \{1\} & \text{when } x > 0 \\ [-1, 1] & \text{when } x = 0 \\ \{-1\} & \text{when } x < 0 \end{cases}$$

Then, the subdifferential of the absolute value function is  $\text{sgn}(x)$  and for all  $\delta \mathbf{w}_h, \mathbf{w}_h, \mathbf{u}_h, \mathbf{v}_h \in \mathbf{X}_h$ , we define a generalization of the partial derivative as

$$\frac{\partial s_h}{\partial \mathbf{u}_h}(\mathbf{u}_h; \boldsymbol{\chi}_h, \boldsymbol{\xi}_h) \cdot (\delta \mathbf{u}_h) = \frac{1}{2} \sum_{S \in \mathcal{S}_h^{(i)}} \int_S [[\boldsymbol{\chi}_h]] : [[\boldsymbol{\xi}_h]] \text{sgn}(\mathbf{u}_h \cdot \mathbf{n}) \, \delta \mathbf{u}_h \cdot \mathbf{n} \, ds$$

Thus, the Jacobian  $\frac{\partial F}{\partial U}$  can be defined as a multi-valued subgradient set. In 1993, Qi and Sun [52] showed how the Newton method extends to this case: any element that belongs to this set represents a valid direction for the Newton correction step. Such a *non-smooth* Newton method was



successfully implemented for the steady Navier-Stokes equations with the discontinuous Galerkin method and upwinding [60].

The multi-valued Jacobian  $\frac{\partial F}{\partial \mathbf{U}}$  is defined for all  $(\boldsymbol{\chi}_h, \mathbf{u}_h, p_h) \in T_h \times V(\mathbf{u}_\Gamma) \times Q_h$ , and  $(\delta \boldsymbol{\chi}_h, \delta \mathbf{u}_h, \delta p_h) \in T_h \times V(0) \times Q_h$   $(\boldsymbol{\xi}_h, \mathbf{v}_h, q_h)$  by

$$\begin{aligned} & \left\langle \frac{\partial F}{\partial \mathbf{U}}(\lambda, (\boldsymbol{\chi}_h, \mathbf{u}_h, p_h)) \cdot (\delta \boldsymbol{\chi}_h, \delta \mathbf{u}_h, \delta p_h), (\boldsymbol{\xi}_h, \mathbf{v}_h, q_h) \right\rangle \\ &= a_1(\boldsymbol{\chi}_h, \mathbf{u}_h; \delta \boldsymbol{\chi}_h, \boldsymbol{\xi}_h) + b_{11}(\boldsymbol{\chi}_h, \mathbf{u}_h; \boldsymbol{\xi}_h, \delta \mathbf{u}_h) \\ & \quad + b_{12}(\boldsymbol{\chi}_h; \delta \boldsymbol{\chi}_h, \mathbf{v}_h) - c(\delta \mathbf{u}_h, \mathbf{v}_h) - d(\mathbf{v}_h, \delta p_h) \\ & \quad - d(\delta \mathbf{u}, q) \end{aligned}$$

where

$$\begin{aligned} a_1(\boldsymbol{\chi}, \mathbf{u}; \delta \boldsymbol{\chi}, \boldsymbol{\xi}) &= \frac{\partial t_h}{\partial \boldsymbol{\chi}}(\mathbf{u}; \boldsymbol{\chi}, \boldsymbol{\xi}) \cdot (\delta \boldsymbol{\chi}) + \frac{\partial a}{\partial \boldsymbol{\chi}}(\boldsymbol{\chi}, \boldsymbol{\xi}) \cdot (\delta \boldsymbol{\chi}) \\ &= \lambda t_{0,h}(\mathbf{u}; \delta \boldsymbol{\chi}, \boldsymbol{\xi}) + s_h(\mathbf{u}; \delta \boldsymbol{\chi}, \boldsymbol{\xi}) + \int_{\partial \Omega} \delta \boldsymbol{\chi} : \boldsymbol{\xi} \max(0, -\mathbf{u}_\Gamma \cdot \mathbf{n}) \, ds \\ & \quad + \frac{a\lambda}{\eta_p} \int_{\Omega} \left( \frac{\partial \kappa}{\partial \boldsymbol{\beta}} \left( \frac{a\lambda}{\eta_p} \boldsymbol{\chi}, 2D(\mathbf{u}) \right) : \delta \boldsymbol{\chi} \right) : \boldsymbol{\xi} \, dx \\ & \quad + \int_{\Omega} \delta \boldsymbol{\chi} : \boldsymbol{\xi} \, dx + \int_{\Omega} \left( \exp' \left( -\frac{a\lambda}{\eta_p} \boldsymbol{\chi} \right) : \delta \boldsymbol{\chi} \right) : \boldsymbol{\xi} \, dx \\ b_{11}(\boldsymbol{\chi}, \mathbf{u}; \boldsymbol{\xi}, \delta \mathbf{u}) &= \lambda t_{0,h}(\delta \mathbf{u}; \boldsymbol{\chi}, \boldsymbol{\xi}) + \lambda \frac{\partial s_h}{\partial \mathbf{u}}(\mathbf{u}; \boldsymbol{\chi}, \boldsymbol{\xi}) \cdot (\delta \mathbf{u}) + b_1(\boldsymbol{\xi}, \delta \mathbf{u}) \\ & \quad + \int_{\Omega} \kappa \left( \frac{a\lambda}{\eta_p} \boldsymbol{\chi}, 2D(\mathbf{u}) \right) : \boldsymbol{\xi} \, dx \\ b_{12}(\boldsymbol{\chi}; \delta \boldsymbol{\chi}, \mathbf{v}) &= \frac{\partial b_2}{\partial \boldsymbol{\chi}}(\boldsymbol{\chi}, \mathbf{v}) \cdot (\delta \boldsymbol{\chi}) \\ &= - \int_{\Omega} \delta \boldsymbol{\chi} : D(\mathbf{v}) \, dx - \int_{\Omega} \left( \exp' \left( \frac{a\lambda}{\eta_p} \boldsymbol{\chi} \right) : \delta \boldsymbol{\chi} \right) : \boldsymbol{\xi} \, dx \end{aligned}$$

and where  $t_{0,h}$  denotes the following linear stress transport operator:

$$\begin{aligned} t_{0,h}(\mathbf{u}_h; \boldsymbol{\chi}_h, \boldsymbol{\xi}_h) &= \sum_{K \in \mathcal{T}_h} \int_K ((\mathbf{u}_h \cdot \nabla) \boldsymbol{\chi}_h) : \boldsymbol{\xi}_h \, dx - \sum_{S \in \mathcal{S}_h^{(i)}} \int_S [[\boldsymbol{\chi}_h]] : \{\{\boldsymbol{\xi}_h\}\} (\mathbf{u}_h \cdot \mathbf{n}) \, ds \\ & \quad + \int_{\Omega} (\boldsymbol{\chi}_h W(\mathbf{u}_h) - W(\mathbf{u}_h) \boldsymbol{\chi}_h) : \boldsymbol{\xi}_h \, dx \end{aligned}$$

Here  $\exp'(\boldsymbol{\chi}) : \delta \boldsymbol{\chi}$  denotes the differential at  $\delta \boldsymbol{\chi}$  of the exponential of a  $d \times d$  matrix. Recall that when  $\boldsymbol{\chi}$  and  $\delta \boldsymbol{\chi}$  commutes, then  $\exp'(\boldsymbol{\chi}) : \delta \boldsymbol{\chi} = \exp(\boldsymbol{\chi}) \delta \boldsymbol{\chi}$  while the general case is more complex.

Also  $\frac{\partial \kappa}{\partial \boldsymbol{\beta}}$  involves the derivatives of eigenvalues and eigenvectors of a  $d \times d$  matrix with respect to the matrix coefficients. Notice that, since  $\kappa$  is linear with respect to its second variable  $\boldsymbol{\gamma}$  we have  $\frac{\partial \kappa}{\partial \boldsymbol{\gamma}}(\boldsymbol{\beta}, \boldsymbol{\gamma}) : \delta \boldsymbol{\gamma} = \kappa(\boldsymbol{\beta}, \delta \boldsymbol{\gamma})$ . A key point of the present implementation of the Newton method is the

exact computation of both  $\exp(\boldsymbol{\chi})$ ,  $\exp'(\boldsymbol{\chi})$ ,  $\kappa(\boldsymbol{\beta}, \boldsymbol{\gamma})$  and  $\frac{\partial \kappa}{\partial \boldsymbol{\beta}}(\boldsymbol{\beta}, \boldsymbol{\gamma})$ . Indeed, these computation can be performed explicitly: Rouvière [54, p. 297] proposes some tools for the derivation of an exponential of a matrix while Hairer and Wanner [25, p. 102] give some formula for computing derivative of eigenvalues and Magnus and Neudecker [41, p. 177] present also the derivative of eigenvectors with respect to the coefficient of a matrix. Kane, Guénette, and Fortin [33, p. 50] proposed some explicit expressions for  $\exp(\boldsymbol{\chi})$  and  $\exp'(\boldsymbol{\chi})$ , based on the `mapple` software: these

expressions contained some errors and we provide here, for completeness, the correct expression in appendix A.1. Appendix A.2 shows that  $\kappa$  is continuous and differentiable with respect to the matrix coefficients and details for the first time how to compute these quantities. Finally, the integrals involving nonlinear expressions are evaluated by a Gauss quadrature formula with six interior nodes in a triangle: this quadrature formula is exact for polynomials which degree is lower or equal to four. Numerical experiments with higher order of quadrature order do not produce any perceptible change in the numerical results.

## 2.4 Euler-Newton continuation algorithm

The aim of the Euler-Newton continuation algorithm is to start from a previous computed solution at a smaller  $\lambda$  (or dimensionless Weissenberg number), perform a prediction by using an Euler scheme (as if  $\lambda$  was a pseudo-time) and then do corrections with the Newton method. This approach allows to reach efficiently high values of the  $\lambda$  parameter.

Let us denote  $U = (\boldsymbol{\chi}_h, \mathbf{u}_h, p_h) \in T_h \times X_h \times Q_h$ , such that the approximate nonlinear problem writes in a concise form  $F(\lambda, U) = 0$ . In this paragraph, we introduce an Euler-Newton continuation algorithm (see e.g. [50, p. 176] or [64]) that contains two nested loops:

**algorithm 1** (*continuation*)

- $n = 0$ : Let  $(\lambda_0, U_0)$  be given. Compute

$$\dot{U}_0 = - \left( \frac{\partial F}{\partial U}(\lambda_0, U_0) \right)^{-1} \frac{\partial F}{\partial \lambda}(\lambda_0, U_0)$$

- $n \geq 0$ : Let  $(\lambda_n, U_n)$  and  $\dot{U}_n$  being known.

- 1) First choose a step  $\Delta\lambda_n$  and set  $\lambda_{n+1} = \lambda_n + \Delta\lambda_n$ .
- 2) Then, perform an Euler prediction by computing

$$w_0 = U_n - \Delta\lambda_n \left( \frac{\partial F}{\partial U}(\lambda_n, U_n) \right)^{-1} \frac{\partial F}{\partial \lambda}(\lambda_n, U_n)$$

- 3) Then, perform a Newton correction step: for all  $k \geq 0$ , with  $W_k$  being known, compute

$$W_{k+1} = W_k - \left( \frac{\partial F}{\partial U}(\lambda_{n+1}, W_k) \right)^{-1} F(\lambda_{n+1}, W_k)$$

At convergence of the correction loop, set  $U_{n+1} = W_\infty$ .

- 4) Finally, compute

$$\dot{U}_{n+1} = - \left( \frac{\partial F}{\partial U}(\lambda_{n+1}, U_{n+1}) \right)^{-1} \frac{\partial F}{\partial \lambda}(\lambda_{n+1}, U_{n+1})$$

The step  $\Delta\lambda_n$  can either be fixed or chosen by adjusting the contraction ratio of the Newton method [50, 64]. The previous algorithm requires the computation of  $\frac{\partial F}{\partial \lambda}$ , that expresses:

$$\begin{aligned} & \left\langle \frac{\partial F}{\partial \lambda}(\lambda, (\boldsymbol{\chi}_h, \mathbf{u}_h, p_h)), (\boldsymbol{\xi}_h, \mathbf{v}_h, q_h) \right\rangle \\ &= t_{0,h}(\mathbf{u}_h; \boldsymbol{\chi}_h, \boldsymbol{\xi}_h) + s_h(\mathbf{u}_h; \boldsymbol{\chi}_h, \boldsymbol{\xi}_h) + \int_{\partial\Omega} \max(0, -\mathbf{u}_\Gamma \cdot \mathbf{n}) \boldsymbol{\chi}_h : \boldsymbol{\xi}_h \, ds \\ &+ \frac{a}{\eta_p} \int_{\Omega} \left( \frac{\partial \kappa}{\partial \boldsymbol{\chi}} \left( \frac{a\lambda}{\eta_p} \boldsymbol{\chi}_h, 2D(\mathbf{u}_h) \right) : \boldsymbol{\chi}_h \right) : \boldsymbol{\xi}_h \, dx \\ &- \frac{a}{\eta_p} \int_{\Omega} \frac{\partial f}{\partial \mu} \left( \frac{a\lambda}{\eta_p}, -\boldsymbol{\chi}_h \right) : \boldsymbol{\xi}_h \, dx - \frac{a}{\eta_p} \int_{\Omega} \frac{\partial f}{\partial \mu} \left( \frac{a\lambda}{\eta_p}, \boldsymbol{\chi}_h \right) : D(\mathbf{v}_h) \, dx \end{aligned}$$

where

$$\frac{\partial f}{\partial \mu}(\mu, \boldsymbol{\chi}) = \begin{cases} \frac{\boldsymbol{\chi}^2}{2} & \text{when } \mu = 0 \\ -\frac{1}{\mu^2} (\exp(\mu\boldsymbol{\chi}) - I) + \frac{1}{\mu} \exp'(\mu\boldsymbol{\chi}) : \boldsymbol{\chi} & \text{otherwise} \end{cases}$$

## 2.5 Automatic adaptive mesh

The anisotropic auto-adaptive mesh feature available in the `Rheolef` free software FEM library [59] has been used in this paper. This feature bases on the free software `bamg` bidimensional anisotropic mesh generator developed by Hecht [27]. Let us first summarize the principle of the adaptive mesh procedure. Let  $\mathcal{T}_h$  be an initial mesh and  $U = (\boldsymbol{\chi}_h, \mathbf{u}_h, p_h) \in T_h \times X_h \times Q_h$  be the solution of the discrete nonlinear problem  $(FV)_h$  associated to the mesh  $\mathcal{T}_h$ . Let  $\phi$  be a *governing field* to be suitably chosen from the solution  $U$ . For a piecewise linear interpolation of  $\phi$ , the interpolation error in the unitary direction  $\mathbf{d} \in \mathbb{R}^2$  is estimated in any element  $K \in \mathcal{T}_h$  by:

$$e_{K,\mathbf{d}} = h_{K,\mathbf{d}}^2 \left| \frac{\partial^2 \phi}{\partial \mathbf{d}^2} \right| \text{ in } K$$

where  $h_{K,\mathbf{d}}$  is the length of  $K$  in the  $\mathbf{d}$  direction and

$$\frac{\partial^2 \phi}{\partial \mathbf{d}^2} = \mathbf{d}^T \mathbf{H}(\phi) \mathbf{d} \quad \text{and} \quad \mathbf{H}(\phi) = \begin{pmatrix} \frac{\partial^2 \phi}{\partial x^2} & \frac{\partial^2 \phi}{\partial x \partial y} \\ \frac{\partial^2 \phi}{\partial x \partial y} & \frac{\partial^2 \phi}{\partial y^2} \end{pmatrix}$$

Here  $\mathbf{H}(\phi)$  denotes the Hessian of  $\phi$ . A possibility to adapt the mesh to the computation of  $\phi$  is to equi-distribute this error, i.e. to make it constant over all triangles and in all directions. Let  $\lambda_1, \lambda_2$  be the eigenvalues of  $\mathbf{H}(\phi)$  and  $\mathbf{d}_1$  and  $\mathbf{d}_2$  the associated eigenvectors:

$$\frac{\partial^2 \phi}{\partial \mathbf{d}_1^2} = \lambda_1 \quad \text{and} \quad \frac{\partial^2 \phi}{\partial \mathbf{d}_2^2} = \lambda_2$$

The error  $e_{K,\mathbf{d}}$  is independent of  $\mathbf{d}$  and  $K$  when there exists a constant  $e_0 > 0$  independent of  $K$

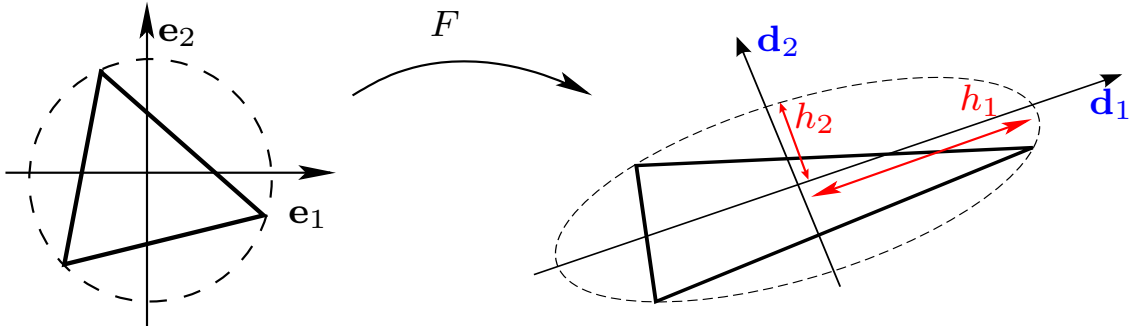


Figure 2: Anisotropic adaptive mesh.

such that  $e_{K,\mathbf{d}_1} = e_{K,\mathbf{d}_2} = e_0$ . This writes equivalently

$$h_{K,\mathbf{d}_1}^2 |\lambda_1| = h_{K,\mathbf{d}_2}^2 |\lambda_2| = e_0, \quad \forall K \in \mathcal{T}_h$$

The constant  $e_0$  represents a global surface density factor: the adapted mesh generator tries to shrink elements in all directions with a factor  $\sqrt{e_0}$  and all the bidimensional element areas are

thus reduced by a factor  $e_0$ . Suppose that  $\mathbf{H}(\phi)$  is non-singular, i.e.  $\lambda_1\lambda_2 \neq 0$ . The constant  $e_0$  being known, our aim is now to build triangles of length  $h_i$  in the  $\mathbf{d}_i$  direction with  $h_i = \sqrt{e_0/|\lambda_i|}$ ,  $i = 1, 2$ . Such a triangle has no privileged direction in a metric such that the two  $h_i\mathbf{d}_i$  vectors,  $i = 1, 2$ , have the same norm. Thus, let us introduce the metric  $\mathbf{M}(\phi)$  tensor that have the same eigenvectors as  $\mathbf{H}(\phi)$  and  $|\lambda_i|$ ,  $i = 1, 2$  as eigenvalues. The induced norm  $\|\cdot\|_M$  satisfies

$$\|h_i\mathbf{d}_i\|_M = h_K \sqrt{\mathbf{d}_i^T \mathbf{M}(\phi) \mathbf{d}_i} = \sqrt{e_0}, \quad i = 1, 2$$

Then, it suffices to build an isotropic mesh in the Riemann space associated to the metric  $\mathbf{M}(\phi)$ : in the Euclidean space, this mesh locally shrinks with a factor  $h_i$  in the  $\mathbf{d}_i$  direction.

It remains to choose a suitable  $\phi$  governing field. Several numerical experiments have led to use the combination of a *free energy* and a *viscous dissipation* term:

$$\phi = \lambda \operatorname{tr} \left( f \left( \frac{a\lambda}{\eta_p}, \boldsymbol{\chi} \right) \right) + \eta_v |D(\mathbf{u})|^2$$

where  $f$  is defined in (7). As both  $\boldsymbol{\chi}_h$  and  $D(\mathbf{u}_h)$  are linear and piecewise discontinuous, the governing field  $\phi$  is also approximated by a piecewise linear and discontinuous function  $\phi_h$ . obtaining its hessian requires then a  $L^2$  projection and two derivations. The  $L^2$  projection of  $\phi_h$  furnishes a piecewise linear and continuous approximation of  $\phi$ , denoted by  $\tilde{\phi}_h$ . The discrete Hessian  $\mathbf{H}_h$  is obtained from  $\tilde{\phi}_h$  by computing first its discrete gradient  $\mathbf{g}_h$ , continuous and piecewise linear, from the variational formula:

$$\int_{\Omega} \mathbf{g}_h \cdot \mathbf{v}_h \, dx = \int_{\Omega} \nabla \tilde{\phi}_h \cdot \mathbf{v}_h \, dx$$

where  $\mathbf{v}_h$  is any continuous piecewise linear vector. Then  $\mathbf{H}_h$  is obtained from the variational formula:

$$\int_{\Omega} \mathbf{H}_h : \boldsymbol{\xi}_h \, dx = \int_{\Omega} D(\mathbf{g}_h) : \boldsymbol{\xi}_h \, dx$$

where  $\boldsymbol{\xi}_h$  is any continuous piecewise linear tensor. Solving a problem using an automatic adaptive mesh is an iterative process, which involves three main steps :

1. Starting from an initial mesh  $\mathcal{T}_h$ , solves the problem by using the Newton method. Let  $U$  be the corresponding solution associated to the mesh  $\mathcal{T}_h$ .
2. From  $U$ , computes the governing field  $\phi_h$ .
3. From the governing field  $\phi_h$ , defined on the mesh  $\mathcal{T}_h$ , generates a totally new mesh, denoted by  $\mathcal{T}_h^{(1)}$ .

Then,  $\mathcal{T}_h^{(1)}$  is used to solve the problem, and so on, until convergence of both the mesh and its associated solution. Hence, the final adapted mesh minimizes the interpolation error for the governing field. This choice of the governing field has been founded to be able to catch accurately the boundary layers and secondary vortex, as showed in the next section.

### 3 Tests on the smoothed driven cavity flow

For the purpose of comparison with previous authors [16, 26], consider the steady bi-dimensional smoothed driven cavity benchmark with  $\Omega = ]0, L[^2$  with  $L > 0$ . The boundary velocity  $\mathbf{u}_\Gamma$  is zero except on the top boundary  $\{y = L\}$  where  $\mathbf{u}_\Gamma(x, L) = (16Ux^2(L-x)^2/L^2, 0)$  with  $U > 0$ . The fluid parameters are  $a = 1$  and  $\eta_p = \eta_v$  and the dimensionless Weissenberg number is  $We = \lambda U/L$ . Despite its simple geometry, this is a very difficult benchmark: to our knowledge, most numerical methods based on the initial formulation failed for  $We \leq 0.1$ . Due to singularities near corners

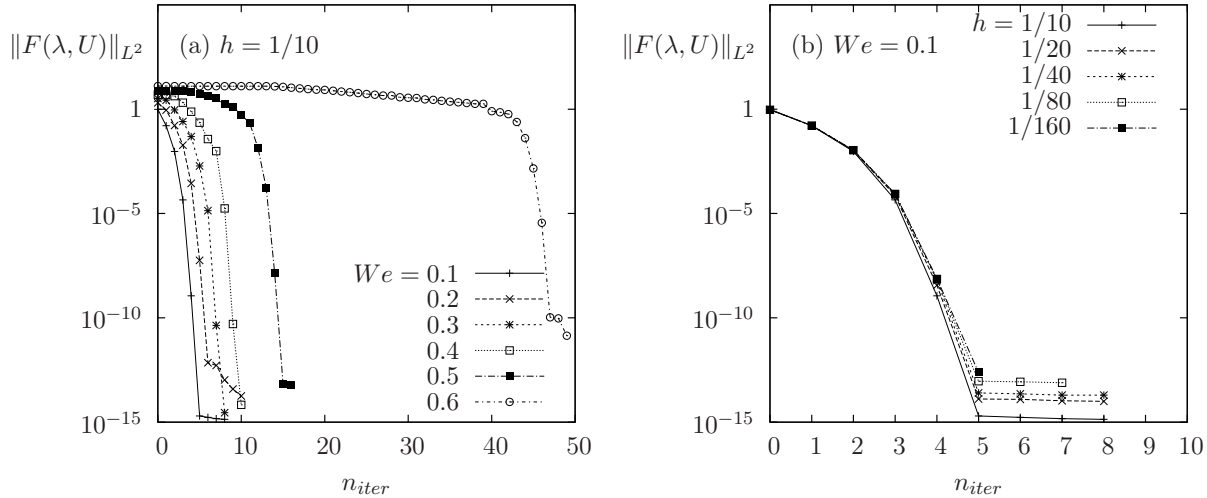


Figure 3: Convergence of the damped Newton algorithm, starting from the solution at  $We = 0$  for the Oldroyd-B problem on the driven cavity with  $\eta_p = \eta_v$ : (a) versus  $We$  for an uniform mesh with  $h = 1/10$ ; (b) versus mesh refinement  $h$  for  $We = 0.1$ .

between the lid and the side walls, the lid-driven cavity may encounter the high  $We$  number problem or offer many challenges in the form of singularity points in the flow. Therefore, it is known as a very stringent test problem for a numerical methods.

Fig. 3.a plots the residual term  $\|F(\lambda, U)\|_{L^2}$  versus the iteration number  $n_{iter}$  of the damped Newton method. The loop is initialized from the Newtonian solution, associated to  $We = 0$  and the solution is then computed *directly* for a specific  $We$ . Observe the quadratic convergence in log scale, up to  $We = 0.5$ . The algorithm is stopped when the machine precision is reached. For the last test case  $We = 0.6$ , the damped strategy still allows the convergence of the algorithm at the price of a larger number of iteration and the loss of the quadratic convergence. In that case, the Euler-Newton continuation algorithm, that restarts from a previous computed solution at a smaller  $We$  is more efficient: we used a Weissenberg step  $\Delta We = 0.1$  in the present computations. Moreover, the Euler-Newton continuation algorithm is more robust and allows to reach solutions at much higher Weissenberg numbers. With this algorithm, each step uses about fives resolution of the Jacobian linear system and the solution at  $We = 1$  can be reached from the solution at  $We = 0$  with about fifty resolutions of linear systems. This convergence property is *mesh-invariant*, as showed by Fig. 3.b (for the mesh-invariance property of nonlinear algorithms, see [59, chap. 8]). This algorithm provides also all the intermediate solutions at  $We = 0.1, \dots, 0.9$ . Such very efficient viscoelastic computations for large Weissenberg numbers can be compared with the thousand of steps involving linear systems and required by all the actual time-dependent approaches for reaching the steady solution [16, 26, 33, 13]. Moreover, the number of time steps required by these methods increases with the Weissenberg number, and also with mesh refinement when non-fully implicit time schemes are used.

The current implementation uses the **Rheolef** free software FEM library [59, 60] that is available as standard package under the Debian and Ubuntu GNU/Linux systems. The Jacobian matrix  $\frac{\partial F}{\partial U}$  is large and sparse: the linear system is solved by a direct method with the help of the parallel and massively distributed memory linear solver **mumps** [2] together with the **scotch** [51] ordering algorithm for minimizing the fill-in of the sparse matrix. For the largest meshes ( $h = 1/80, 1/160$  and the adaptive meshes), the computations is run with 32 processors on a BullX DLC supercomputer (Bull Newsca) composed of nodes having two intel sandy-bridge processors and connected to a FDR infiniband non-blocking low latency network. The computation of a whole branch of solutions is performed in less than one hour of real time.

$h$	$We_{\max}$
1/20	3.74
1/40	2.19
1/80	2.21
1/160	2.08

$h_{\min}$	$We_{\max}$	$We_c$
$10^{-2}$	3.13	2.33
$5 \times 10^{-3}$	2.78	2.03

Table 1: The Oldroyd-B problem on the driven cavity with  $\eta_p = \eta_v$ . Maximal and critical Weissenberg number versus mesh refinement: (left) uniform mesh ; (right) adapted mesh.

Table 1 (left) groups the maximal Weissenberg number, denoted as  $We_{\max}$ , reached by the Euler-Newton continuation algorithm: for higher  $We$ , the algorithm stops, due to a singular solution where the Jacobian matrix  $\frac{\partial F}{\partial U}$  is non-invertible. When such a singularity occurs in the continuation algorithm, the Weissenberg step is divided by two and the iteration restarted. The Weissenberg step is limited to  $10^{-7}$ . When using adaptive mesh, we observe that the Euler-Newton continuation algorithm is able to jump behind the singular point and continues its progression on a branch of solution until a second singular point is reached near  $We = 3$ . In that case, the determinant of the Jacobian matrix exhibits a change of sign after the first singular point (see e.g. [64]). The Weissenberg number where this change of sign occurs is denoted as  $We_c$  on table 1 (right). Observe that for the finest uniform mesh ( $h = 1/160$ ), the singular point is  $We_c = 2.08$  and for the finest adapted one,  $We_c = 2.03$ . Then  $We_c$  seems to become mesh insensitive with mesh refinement. A deeper analysis of singular points is planned for future works: it requires more advanced tools than the simple continuation Euler-Newton algorithm. The first and second singular points could be e.g. bifurcation points associated to a loss of stationarity of the solution: for larger  $We$ , the solution becomes non-stationary, as suggested by time-dependent simulations (see e.g. [16], Fig. 8). Pakdel, Spiegelberg and McKinley also showed by experimental observations [48] for the motion of viscoelastic fluids in the lid-driven cavity geometry that, at large Weissenberg numbers, the fluid motion becomes unstable and a three-dimensional flow develops.

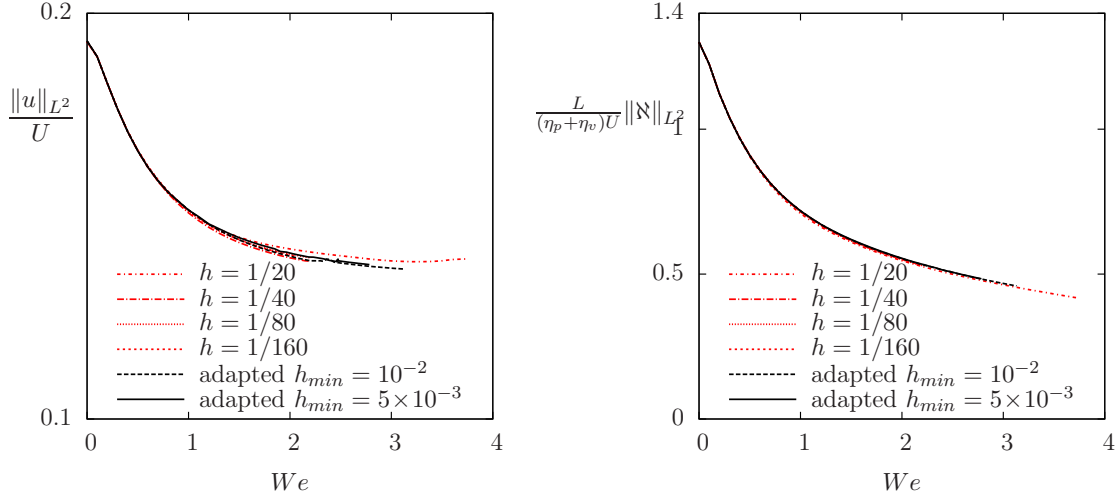


Figure 4: The Oldroyd-B problem on the driven cavity with  $\eta_p = \eta_v$ . Norms of the solution versus  $We$ .

Fig. 4 plots the  $L^2$  norm of the velocity and the log-conformation tensor: observe the good convergence of these quantities versus mesh refinement. There are five uniform meshes from  $h = 1/20$  to  $h = 1/160$  and two adapted meshes with  $h_{\min} = 10^{-2}$  and  $5 \times 10^{-3}$ .

Figs. 5 and 6 show the adapted meshes and stream isovalues of the function for  $We = 1, 2$  and 3. The stream function  $\varphi$  is defined as the unique function that satisfies  $-\Delta\varphi = \partial_y u_x - \partial_x u_y$  in  $\Omega$  with  $\varphi = 0$  on  $\partial\Omega$ . Ten negative and fifteen positive equi-spaced isolines are represented on each plot. Observe that viscoelastic effects break the symmetry observed for the velocity field of cavity flows of viscous Newtonian fluids at zero Reynolds number. At low Weissenberg number, the flow remains two-dimensional but the center of the primary recirculating vortex in the cavity shifts progressively upstream (left). These results are qualitatively in agreement with experimental results [48]. Notice also that the inertial effects for viscous Newtonian fluids (i.e.  $We = 0$  and  $Re > 0$ ) has opposite effects (see e.g. [60, part 2]): the center of the primary recirculating vortex in the cavity shifts downstream (right).

$x_m$	$y_m$	reference
0.439	0.816	Pan, Hao & Glowinski [49]
0.433	0.803	Su, Ouyang, Wang, Yang & Zhou [65]
0.429	0.818	present

Table 2: The Oldroyd-B problem on the driven cavity with  $\eta_p = \eta_v$ . Comparison of the dimensionless main vortex center position for  $We = 1$  with others authors.

Furthermore, our results are compared quantitatively with respect to the previous works: the location of the primary vortex center for  $We = 1$  are listed in table 2. Our results are evaluated comparing with the results of time-dependent flow using both a finite element method [49] and a lattice Boltzmann method [65]. It is found that the results of our steady computations are consistent with those of these authors.

Figs. 7 and 8 show zooms on the left and right secondary vortex. While the main vortex moves from left to right when  $We$  increases, the left vortex grows and the right one decreases in activity. Notice that this is also in opposition with inertial effects for viscous Newtonian fluids.

$We$	main			left			right		
	$x_m$	$y_m$	$\varphi_{\min}$	$x_l$	$y_l$	$\varphi_{\max}$	$x_r$	$y_r$	$\varphi_{\max}$
1	0.429	0.818	-0.0619	0.0364	0.0388	$1.31 \times 10^{-6}$	0.9637	0.0355	$9.97 \times 10^{-7}$
2	0.386	0.828	-0.0555	0.0394	0.0411	$1.58 \times 10^{-6}$	0.9663	0.0363	$7.07 \times 10^{-7}$
3	0.335	0.824	-0.0531	0.0485	0.0477	$3.22 \times 10^{-6}$	0.9631	0.0347	$7.66 \times 10^{-7}$

Table 3: The Oldroyd-B problem on the driven cavity with  $\eta_p = \eta_v$ . Dimensionless main and secondary vortex center position and activity for  $We = 1, 2$  and 3.

Table 3 groups the main and secondary vortex center position and activity for  $We = 1, 2$  and 3. These values are provided future cross validation purpose. Observe that the main vortex goes left and decreases in activity while the center of the left secondary vortex goes up and right and its activity increases. Also, the center of the right secondary vortex roughly stays in place while its activity remains constant. Finally, Fig. 9 plots the cut of the first component  $u_x$  of the velocity and the  $\chi_{xx}$  component along the  $x = 1/2$  vertical axis, as computed with the adaptive mesh. The computations with the finest uniform mesh ( $h = 1/160$ ) gives similar results: it is not showed here, as the difference is not graphically perceptible. Observe the excellent quantitative agreement with both computations obtained by Hao and Pan [26] and Fattal and Kupferman [16].

## Conclusion

The new log-conformation formulation of viscoelastic fluid flows presented in this paper allows a direct steady numerical resolution by a Newton method. Moreover, the use an exact divergence

free finite element method for velocity-pressure approximation and a discontinuous Galerkin up-winding treatment for stresses leads to a robust discretization. A demonstration is provided by the computation of steady solutions at high Weissenberg numbers for the difficult benchmark of the lid driven cavity flow. Numerical results are in good agreement, both qualitatively with experiment measurements on real viscoelastic flows, and quantitatively with computations performed by others authors. The numerical algorithm is thus robust. It is also very efficient, as it requires few and mesh-invariant number of linear systems resolution to reach solutions at high Weissenberg number. An adaptive mesh procedure is also proposed, in order to catch accurately both boundary layers and main and secondary vortex.

We provide new data for future cross validation purpose and point out the existence of a singular point near  $We = 2$ , where the determinant of the Jacobian vanishes and then exhibits a change of sign. This singular point has been founded quite robust with mesh refinement. As suggested by both experimental measurements and time-dependent simulations, it could be a bifurcation points associated to a loss of stationarity of the solution. The analysis of this situation by a steady approach is also possible by the tools of the bifurcation theory. In 2009, a pioneer work was performed in this direction by Howell [28] and it should be carried on in the context of the log-conformation formulation.

There are many geometries that could be explored by this approach: contractions, as in the previous reference, and flow around obstacles are interesting benchmarks, while experimental measurements are also available. The present log-conformation formulation extends naturally to more complex viscoelastic fluid models, such as Phan-Thien and Tanner, Giesekus or elastoviscoplastic one [57, 58]. The integration of the Gordon-Schowalter derivative parameter in the present work also open the door of the numerical modeling of liquid crystals, fiber suspension or active fluid.



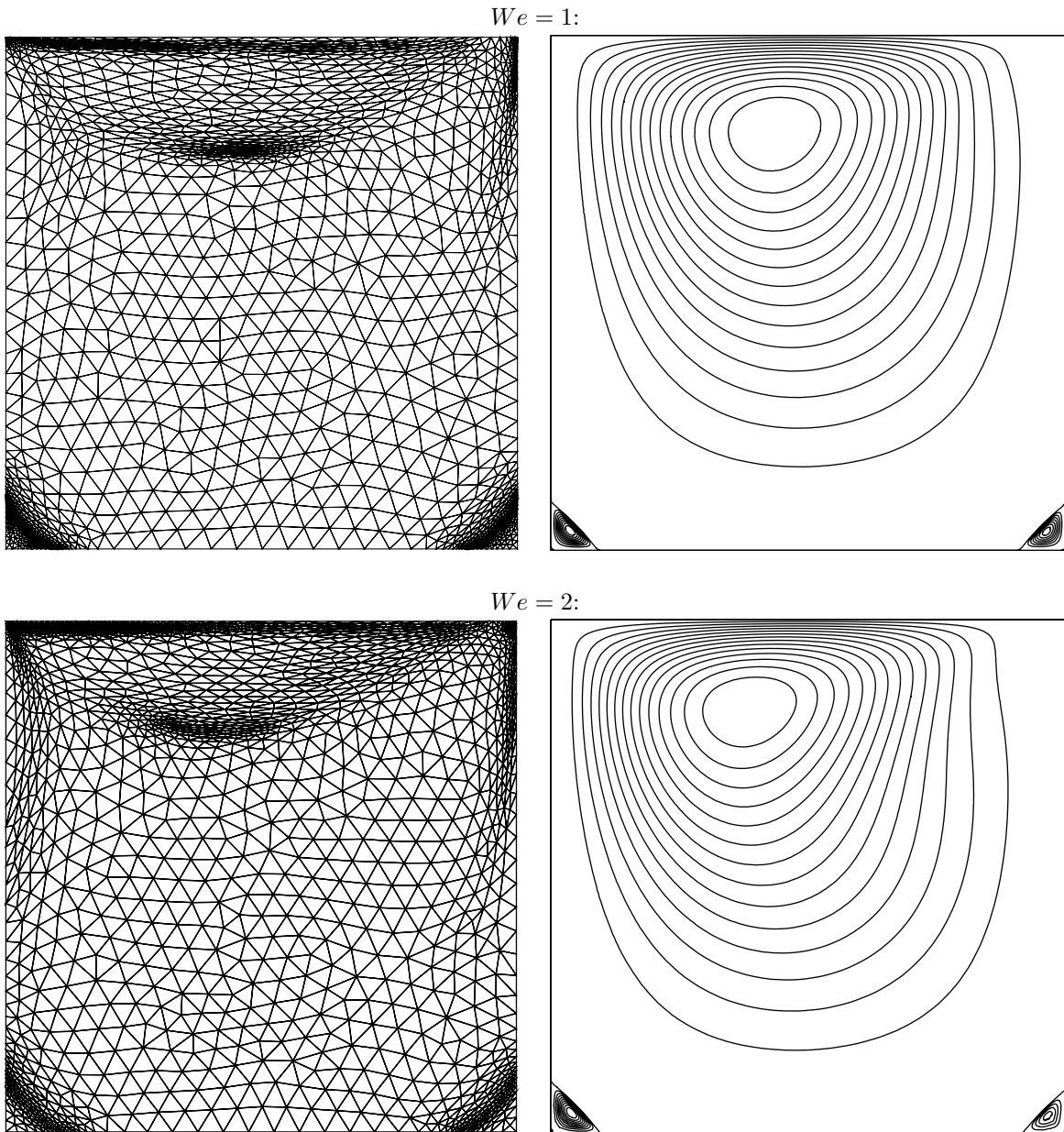


Figure 5: The Oldroyd-B problem on the driven cavity with  $\eta_p = \eta_v$ . Adapted mesh and stream function isovalues for  $We = 1$  and 2.

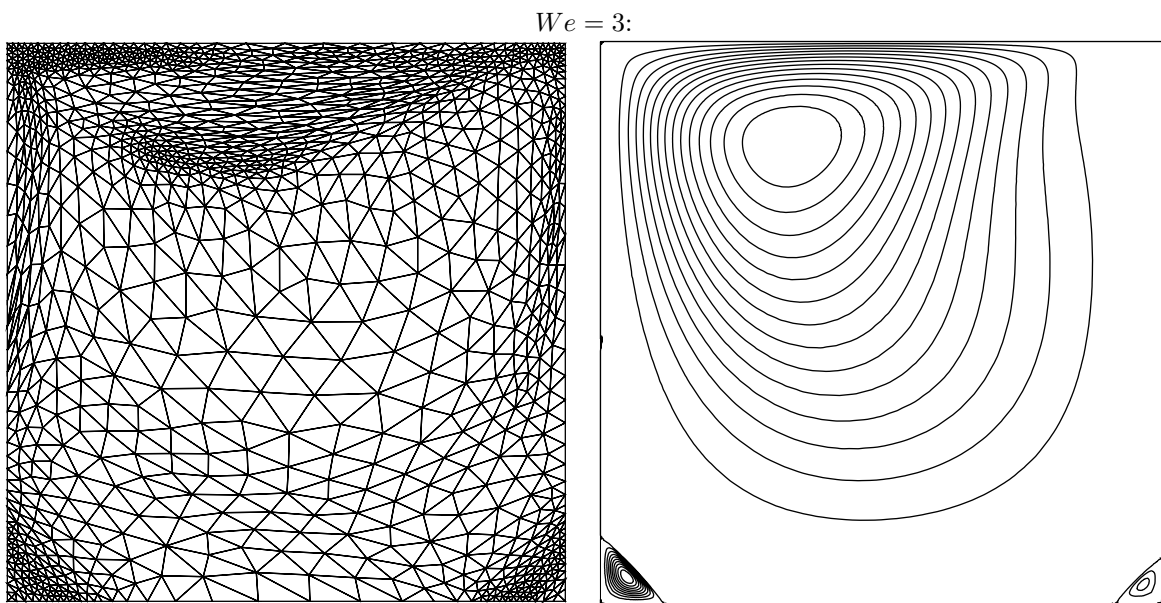


Figure 6: The Oldroyd-B problem on the driven cavity with  $\eta_p = \eta_v$ . Adapted mesh and stream function isovalues for  $We = 3$ .

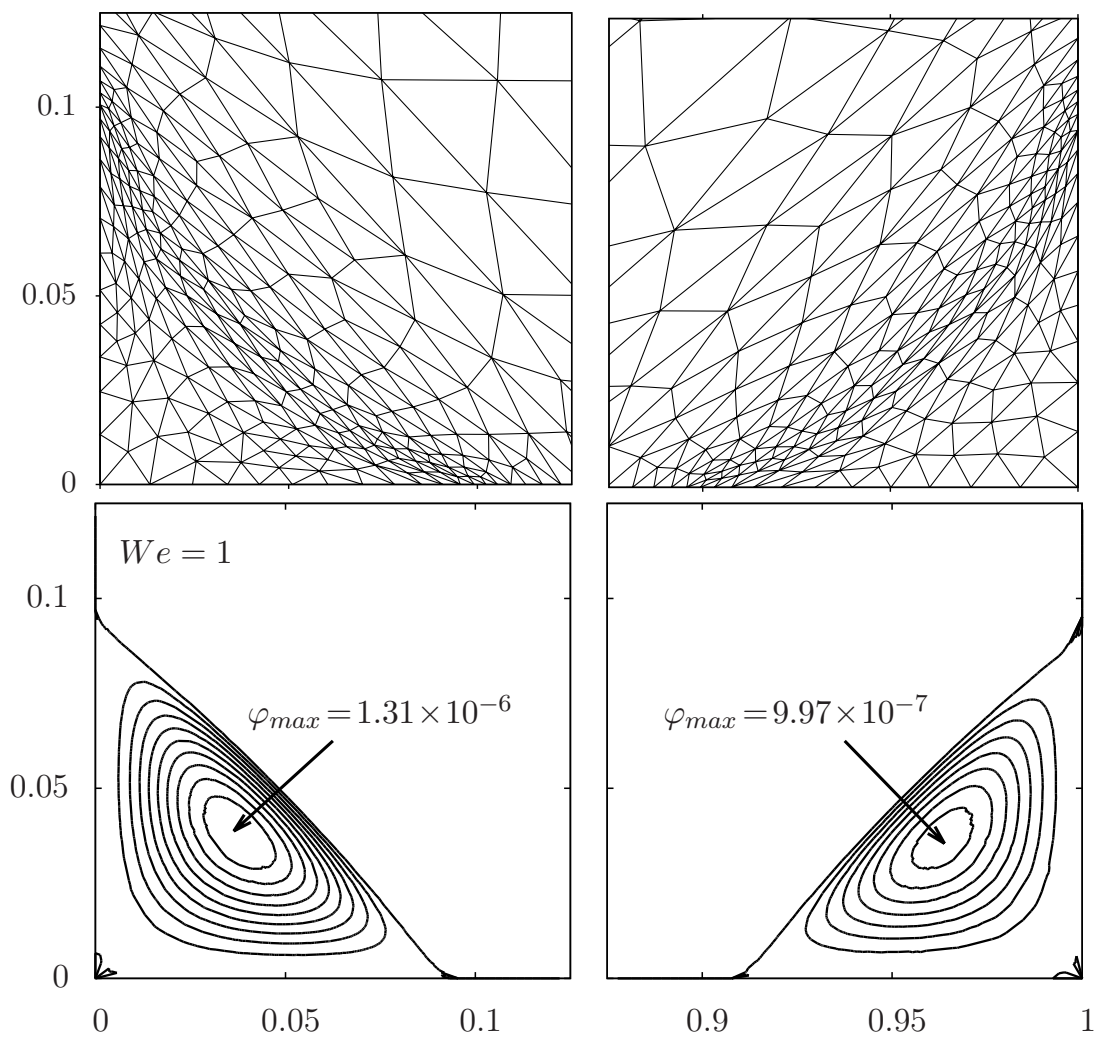


Figure 7: The Oldroyd-B problem on the driven cavity with  $\eta_p = \eta_v$ . Zoom around vortex for  $We = 1$ .

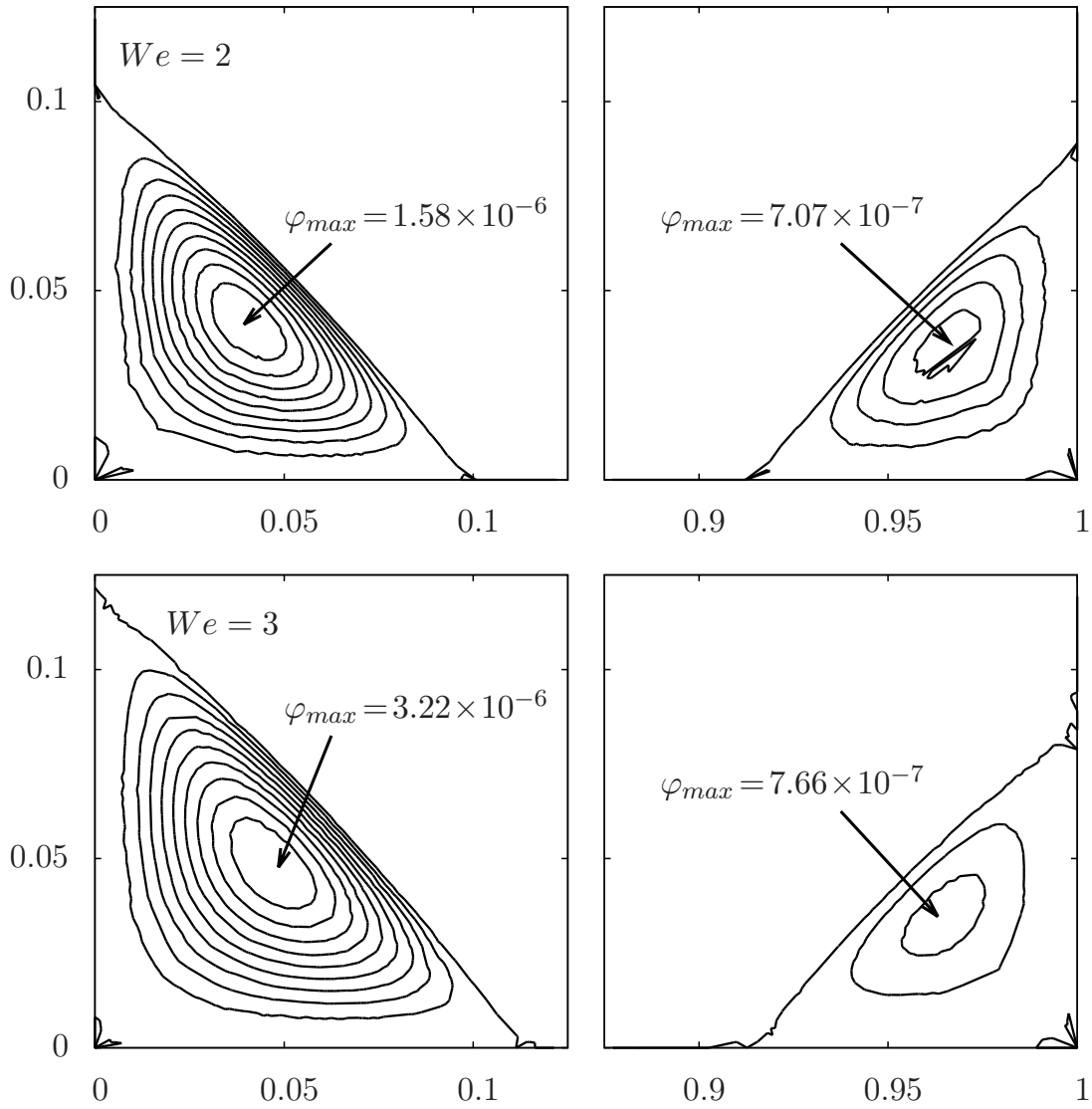


Figure 8: The Oldroyd-B problem on the driven cavity with  $\eta_p = \eta_v$ . Zoom around vortex for  $We = 2$  and 3.

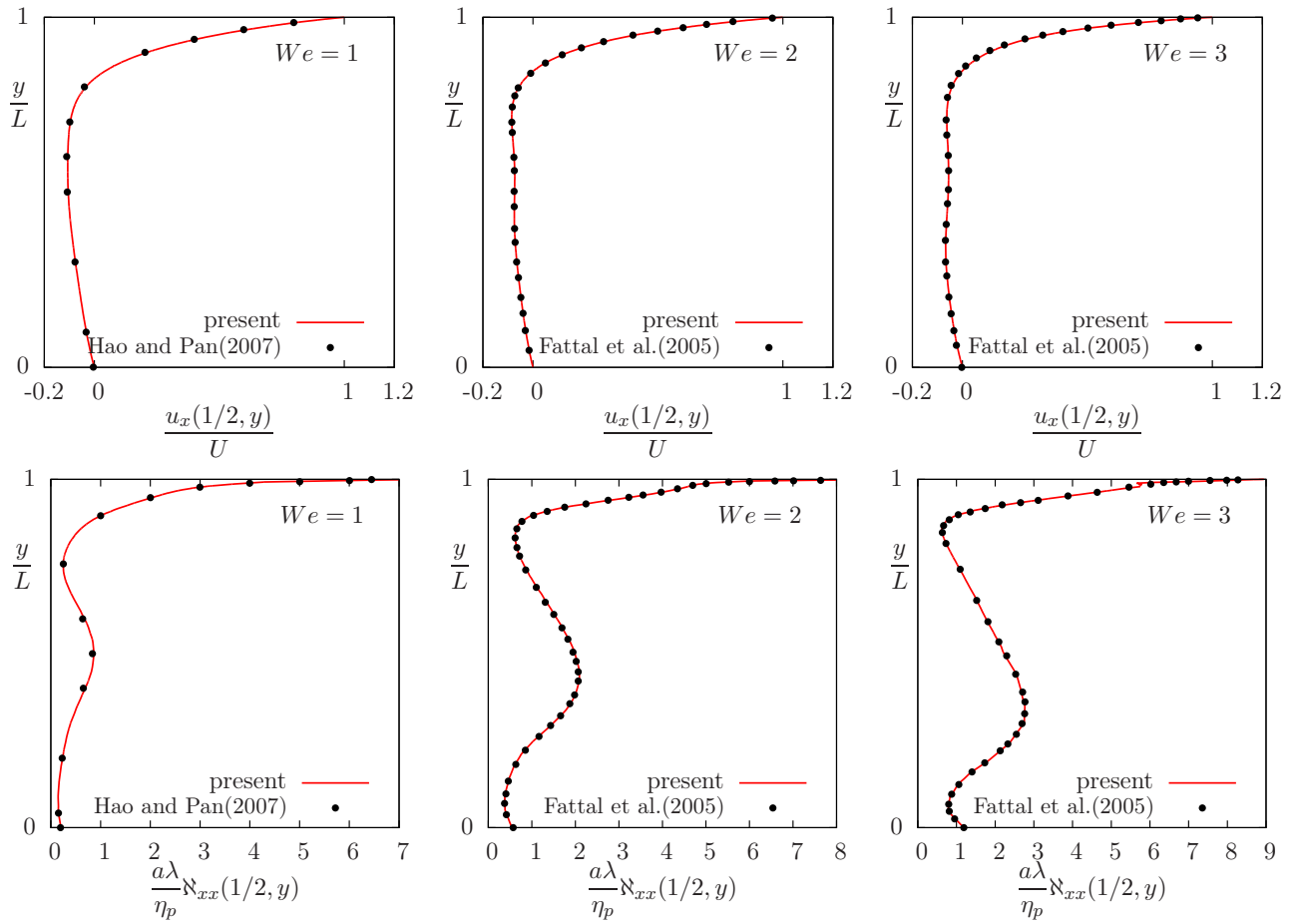


Figure 9: The Oldroyd-B problem on the driven cavity with  $\eta_p = \eta_v$ . Cuts along the  $x = 1/2$  vertical line: (top)  $u_x(1/2, y)$ ; (bottom)  $\chi_{xx}(1/2, y)$ . Comparisons with results obtained by Hao and Pan [26], Fig. 2 for  $We = 1$  and by Fattal and Kupferman [16], Figs. 7 and 10 for  $We = 2$  and 3, respectively.

## References

- [1] A. M. Afonso, M. Oliveira, P. J. Oliveira, M. A. Alves, and F. T. Pinho. *The finite-volume method in computational rheology*, chapter 7, pages 141–170. In-tech publisher, 2012.
- [2] P. Amestoy, A. Buttari, A. Guermouche, J.-Y. L’Excellent, and B. Ucar. *Multifrontal massively parallel solver (MUMPS). User’s guide. Version 4.10.0*. CERFACS, CNRS, INPT(ENSEEIH)-IRIT and INRIA, France, 2011.
- [3] D. N. Arnold and J. Qin. Quadratic velocity/linear pressure Stokes elements. *Adv. Comput. Meth. Partial Diff. Eqn.*, 7:28–34, 1992.
- [4] J. Baranger and D. Sandri. Finite element approximation of viscoelastic fluid flow: existence of approximate solutions and error bounds. part i. discontinuous constraints. *Numer. Math.*, 63:13–27, 1992.
- [5] R. Bird, R. C. Armstrong, and O. Hassager. *Dynamics of polymeric liquids. Volume 2. Kinetic theory*. Wiley, New-York, 1987.
- [6] S. Boyaval. *Modélisation mathématique et simulation numérique en science des matériaux*. PhD thesis, Université Paris Est, 2009.
- [7] S. Boyaval, T. Lelièvre, and C. Mangoubi. Free-energy-dissipative schemes for the Oldroyd-B model. *ESAIM Math. Model. Numer. Anal.*, 43(03):523–561, 2009.
- [8] F. Brezzi. On the existence, uniqueness and approximation of saddle-point problems arising from Lagrangian multipliers. *RAIRO - Anal. Num.*, 8(2):129–151, 1974.
- [9] F. Brezzi and M. Fortin. *Mixed and hybrid finite element methods*. Springer, 1991.
- [10] P. G. Ciarlet, editor. *Handbook of numerical analysis. Volume 16. Numerical methods for non-Newtonian fluids*. Elsevier, 2011.
- [11] O. M. Coronado, D. Arora, M. Behr, and M. Pasquali. A simple method for simulating general viscoelastic fluid flows with an alternate log-conformation formulation. *J. Non-Newt. Fluid Mech.*, 147(3):189–199, 2007.
- [12] H. Damanik. *FEM simulation of non-isothermal viscoelastic fluids*. PhD thesis, Univ. Dortmund, Germany, 2011.
- [13] H. Damanik, J. Hron, A. Ouazzi, and S. Turek. A monolithic FEM approach for the log-conformation reformulation (LCR) of viscoelastic flow problems. *J. Non-Newt. Fluid Mech.*, 165(19):1105–1113, 2010.
- [14] D. A. di Pietro and A. Ern. *Mathematical aspects of discontinuous Galerkin methods*. Springer, 2012.
- [15] R. Fattal and R. Kupferman. Constitutive laws for the matrix-logarithm of the conformation tensor. *J. Non-Newt. Fluid Mech.*, 123(2):281–285, 2004.
- [16] R. Fattal and R. Kupferman. Time-dependent simulation of viscoelastic flows at high Weissenberg number using the log-conformation representation. *J. Non-Newt. Fluid Mech.*, 126(1):23–37, 2005.
- [17] E. Fernández-Cara, F. Guillén, and R. R. Ortega. Some theoretical results concerning non-Newtonian fluids of the Oldroyd kind. *Ann. Scuola Norm. Sup. Pisa Cl. Sci.*, 26(1):1–29, 1998.
- [18] S. M. Fielding, D. Marenduzzo, and M. E. Cates. Nonlinear dynamics and rheology of active fluids: simulations in two dimensions. *Phys. Rev. E*, 83:041910, 2011.

- [19] A. Fortin and A. Zine. An improved GMRES method for solving viscoelastic fluid flow problems. *J. Non-Newtonian Fluid Mech.*, 42(1–2):1–18, 1992.
- [20] M. Fortin and A. Fortin. A new approach for the FEM simulation of viscoelastic flows. *J. Non-Newtonian Fluid Mech.*, 32(3):295–310, 1989.
- [21] M. Fortin and R. Pierre. On the convergence of the mixed method of Crochet and Marchal for viscoelastic flows. *Comp. Meth. Appl. Mech. Engrg.*, 73(3):341–350, 1989.
- [22] V. Girault and P. A. Raviart. *Finite element methods for the Navier-Stokes equations. Theory and algorithms*. Springer, 1986.
- [23] R. J. Gordon and W. R. Schowalter. Anisotropic fluid theory: a different approach to the dumbbell theory of dilute polymer solutions. *J. Rheol.*, 16:79–97, 1972.
- [24] C. Guillopé and J. C. Saut. Résultats d’existence pour les fluides viscoélastiques à loi de comportement de type différentiel. *C. R. Acad. Sci. Paris, Sér. 1*, 305(11):489–492, 1987.
- [25] E. Hairer and G. Wanner. Polycopié genevois d’analyse numérique. Technical report, Université de Genève, Suisse, 2006.
- [26] J. Hao and T.-W. Pan. Simulation for high Weissenberg number viscoelastic flow by a finite element method. *Appl. Math. Lett.*, 20(9):988–993, 2007.
- [27] F. Hecht. *BAMG: bidimensional anisotropic mesh generator*, 2006. <http://www.ann.jussieu.fr/~hecht/ftp/bamg>.
- [28] J. S. Howell. Dual-mixed finite element approximation of Stokes and nonlinear Stokes problems using trace-free velocity gradients. *J. Comput. Appl. Math.*, 231:780–792, 2009.
- [29] D. Hu and T. Lelièvre. New entropy estimates for the Oldroyd-B model and related models. *Commun. Math. Sci.*, 5(4):909–916, 2007.
- [30] M. A. Hulsen. A sufficient condition for a positive definite configuration tensor in differential models. *J. Non-Newton. Fluid Mechanics*, 38(1):93–100, 1990.
- [31] M. A. Hulsen, R. Fattala, and R. Kupferman. Flow of viscoelastic fluids past a cylinder at high Weissenberg number: stabilized simulations using matrix logarithms. *J. of Non-Newtonian Fluid Mech.*, 127:27–39, 2005.
- [32] M. W. Johnson and D. Segalman. A model for viscoelastic fluid behavior which allows non-affine deformation. *J. Non-Newtonian Fluid Mech.*, 2:255–270, 1977.
- [33] A. Kane, R. Guénette, and A. Fortin. A comparison of four implementations of the log-conformation formulation for viscoelastic fluid flows. *J. Non-Newton. Fluid Mech.*, 164(1):45–50, 2009.
- [34] R. Keunings. On the high Weissenberg number problem. *J. Non-Newton. Fluid Mech.*, 20:209–226, 1986.
- [35] R. Kupferman, C. Mangoubi, and E. S. Titi. A Beale-Kato-Majda breakdown criterion for an Oldroyd-B fluid in the creeping flow regime. *submitted*, 2014.
- [36] Y. Kwon and A. I. Leonov. Stability constraints in the formulation of viscoelastic constitutive equations. *J. Non-Newton. Fluid Mech.*, 58(1):25–46, 1995.
- [37] Y.-L. Lee, J. Xu, and C.-S. Zhang. Stable finite element discretizations for viscoelastic flow models. In P. G. Ciarlet and J.-L. Lions, editors, *Handbook of numerical analysis. Volume 16. Numerical methods for non-Newtonian fluids*, chapter 4, pages 371–432. Elsevier, 2011.

- [38] F.-H. Lin, C. Liu, and P. Zhang. On hydrodynamics of viscoelastic fluids. *Comm. Pure Appl. Math.*, 58(11):1437–1471, 2005.
- [39] P. L. Lions and N. Masmoudi. Global solutions for some Oldroyd models of non-Newtonian flows. *Chinese Annals of Mathematics, Series B*, 21(2):131–146, 2000.
- [40] G. G. Lipscomb, M. M. Denn, D. U. Hur, and D. V. Boger. The flow of fiber suspensions in complex geometries. *J. Non-Newton. Fluid Mech.*, 26(3):297–325, 1988.
- [41] J. R. Magnus and H. Neudecker. *Matrix differential calculus with applications in statistics and econometrics*. Wiley, New-York, third edition, 2007.
- [42] C. Mangoubi. *Analytical and numerical problems in the computation of the flow of viscoelastic fluids*. PhD thesis, Hebrew University, Kisluy, Israel, 2008.
- [43] J. M. Marchal and M. J. Crochet. A new mixed finite element for calculating viscoelastic flow. *J. Non-Newtonian Fluid Mech.*, 26:77–144, 1987.
- [44] Maxima. Maxima, a computer algebra system, 2013. <http://maxima.sourceforge.net>.
- [45] J. G. Oldroyd. On the formulation of rheological equations of states. *Proc. Roy. Soc. London A*, 200:523–541, 1950.
- [46] H. C. Öttinger. *Beyond equilibrium thermodynamics*. Wiley, 2005.
- [47] R. Owens and T. Phillips. *Computational rheology*. Imperial college press, London, UK, 2002.
- [48] P. Pakdel, S. H. Spiegelberg, and G. H. McKinley. Cavity flows of elastic liquids: two-dimensional flows. *Phys. Fluids*, 9(11):3123, 1997.
- [49] T.-W. Pan, J. Hao, and R. Glowinski. On the simulation of a time-dependent cavity flow of an Oldroyd-B fluid. *Int. J. Numer. Meth. Fluids*, 60(7):791–808, 2009.
- [50] J.-C. Paumier. *Bifurcation et méthodes numériques. Applications aux problèmes elliptiques semi-linéaires*. Masson, Paris, 1997.
- [51] F. Pellegrini. *PT-Scotch and libscotch 5.1 user’s guide*. Université de Bordeaux and INRIA, France, 2010.
- [52] L. Qi and J. Sun. A nonsmooth version of Newton’s method. *Math. Prog.*, 58(1-3):353–367, 1993.
- [53] M. Renardy. Existence of slow steady flows of viscoelastic fluids with differential constitutive equations. *Z. Angew. Math. u. Mech.*, 65(9):449–451, 1985.
- [54] F. Rouvière. *Petit guide de calcul différentiel à l’usage de la licence et de l’agrégation*. Casini, Paris, second edition, 2003.
- [55] P. Saramito. Numerical simulation of viscoelastic fluid flows using incompressible finite element method and a  $\theta$ -method. *M2AN*, 28(1):1–35, 1994.
- [56] P. Saramito. Efficient simulation of nonlinear viscoelastic fluid flows. *J. Non Newtonian Fluid Mech.*, 60:199–223, 1995.
- [57] P. Saramito. A new constitutive equation for elastoviscoplastic fluid flows. *J. Non Newtonian Fluid Mech.*, 145(1):1–14, 2007.
- [58] P. Saramito. A new elastoviscoplastic model based on the Herschel-Bulkley viscoplasticity. *J. Non Newtonian Fluid Mech.*, 158(1-3):154–161, 2009.
- [59] P. Saramito. *Efficient C++ finite element computing with Rheolef*. CNRS and LJK, 2013. <http://cel.archives-ouvertes.fr/cel-00573970>.



- [60] P. Saramito. *Efficient C++ finite element computing with Rheolef: volume 2: discontinuous Galerkin methods*. CNRS and LJK, 2013. <http://cel.archives-ouvertes.fr/cel-00863021>.
- [61] P. Saramito. *Méthodes numériques en fluides complexes : théorie et algorithmes*. CNRS-CCSD, 2013. <http://cel.archives-ouvertes.fr/cel-00673816>.
- [62] P. Saramito and J.-M. Piau. Flow characteristics of viscoelastic fluids in an abrupt contraction by using numerical modeling. *J. Non Newtonian Fluid Mech.*, 52:263–288, 1994.
- [63] L. R. Scott and M. Vogelius. Norm estimates for a maximal right inverse of the divergence operator in spaces of piecewise polynomials. *M2AN*, 19(1):111–143, 1985.
- [64] R. Seydel. *Practical bifurcation and stability analysis*. Springer, third edition, 2010.
- [65] J. Su, J. Ouyang, X. Wang, B. Yang, and W. Zhou. Lattice Boltzmann method for the simulation of viscoelastic fluid flows over a large range of Weissenberg numbers. *J. Non-Newton. Fluid Mech.*, 194:42–59, 2013.
- [66] C. Taylor and P. Hood. A numerical solution of the Navier-Stokes equations using the finite element technique. *Comput. Fluids*, 1(1):73–100, 1973.
- [67] P. Wapperom and M. A. Hulsen. Thermodynamics of viscoelastic fluids: the temperature equation. *J. Rheol.*, 42:999, 1998.
- [68] S. Zhang. A new family of stable mixed finite elements for the 3d Stokes equations. *Math. Comput.*, 74(250):543–554, 2005.

## A Appendices

This appendix groups explicit computations of some complex expressions, nammely the exponential of a matrix, the  $\kappa$  function and their derivatives with respect to coefficient matrix.

### A.1 The matrix exponential and its derivatives

The present work uses the free software formal calculus system `maxima` [44]. With this system, the computation of the exponential of a  $2 \times 2$  symmetric matrix writes:

```
load(linearalgebra);
domxexpt : false;
chi : matrix([a,b],[b,c]);
exp_chi : factor(matrixexp(chi));
```

The derivative  $\exp'(\chi)$  of this expression with respect to the coefficients of the matrix  $\chi$  are then treated without any difficulty by this formal calculus system. Notice that Kane, Guénette, and Fortin [33, p. 50] proposed some explicit expressions for  $\exp(\chi)$  and  $\exp'(\chi)$ , based on the `mapple` software: these expressions contained some errors and, for completeness, the correct expression are provided here.

$$\chi = \begin{pmatrix} a & b \\ b & c \end{pmatrix}, \quad \exp(\chi) = \alpha_2 \begin{pmatrix} \alpha_4 + \frac{(a-c)\alpha_3}{\alpha_1} & \frac{2b\alpha_3}{\alpha_1} \\ \frac{2b\alpha_3}{\alpha_1} & \alpha_4 - \frac{(a-c)\alpha_3}{\alpha_1} \end{pmatrix}$$

where  $\alpha_1 = \sqrt{(a-c)^2 + 4b^2}$ ,  $\alpha_2 = \exp((a+c)/2)$ ,  $\alpha_3 = \sinh(\alpha_1/2)$ , and  $\alpha_4 = \cosh(\alpha_1/2)$ . Notice that the expression in [33] for  $\exp'(\chi)$  should also be fixed in a similar way.

Observe that the obtained expression degenerates when both  $a = c$  and  $b = 0$ , i.e. when the matrix is proportional to the identity. In that case  $\chi = aI$  and  $\exp(\chi) = \exp(a)I$ . This possible degeneracy is decided when both  $|a - c| < \varepsilon_m$  and  $|b| < \varepsilon_m$  where  $\varepsilon_m$  stands for the machine epsilon, i.e. the higher positive floating number such that  $1 + \varepsilon_m = 1$ . Finally, the expressions produced by `maxima` are simplified and optimized in an automatic way: they are then formatted in `fortran`, `C` or `C++` languages for a direct use by the Euler-Newton continuation algorithm.

## A.2 The $\kappa$ function and its derivatives

Magnus and Neudecker [41, p. 177] showed that the eigenvalues and eigenvectors are differentiable provided that eigenvalues are simple. Otherwise, when there is multiple eigenvalues, there is a serious problem. Let us study this difficulty by considering the  $2 \times 2$  matrix function:

$$\beta(\varepsilon, \delta) = \begin{pmatrix} \alpha + \varepsilon & \delta \\ \delta & \alpha - \varepsilon \end{pmatrix}$$

where  $\alpha$  is some fixed constant and  $\varepsilon$  and  $\delta$  are two variables at the vicinity of zero. The two eigenvalues and the two associated unnormalized eigenvectors are

$$\beta_{\pm} = \alpha \pm \sqrt{\varepsilon^2 + \delta^2} \quad \text{and} \quad \mathbf{v}_{\pm} = \begin{pmatrix} 1 \\ -\left(\frac{\varepsilon}{\delta}\right) \pm \sqrt{1 + \left(\frac{\varepsilon}{\delta}\right)^2} \end{pmatrix}$$

Both eigenvalues are continuous in  $\varepsilon$  and  $\delta$  but not differentiable: the conical surface formed by the eigenvalues has a singularity at  $(\varepsilon, \delta) = (0, 0)$  (see Fig. 10.a). For instance

$$\frac{\partial \beta_{\pm}}{\partial \varepsilon} = \pm \left( 1 + \left( \frac{\delta}{\varepsilon} \right)^2 \right)^{-\frac{1}{2}}$$

For a fixed ratio  $c = \delta/\varepsilon$  however, we can pass through  $(0, 0)$  without noticing the singularity, but the derivative depends upon  $c$ . Thus, the derivative  $\frac{\partial \beta_{\pm}}{\partial \varepsilon}$  are multi-valued in  $(0, 0)$  and the two eigenvalues are not derivable at the origin. Notice that the two eigenvectors depends upon  $c$  only.

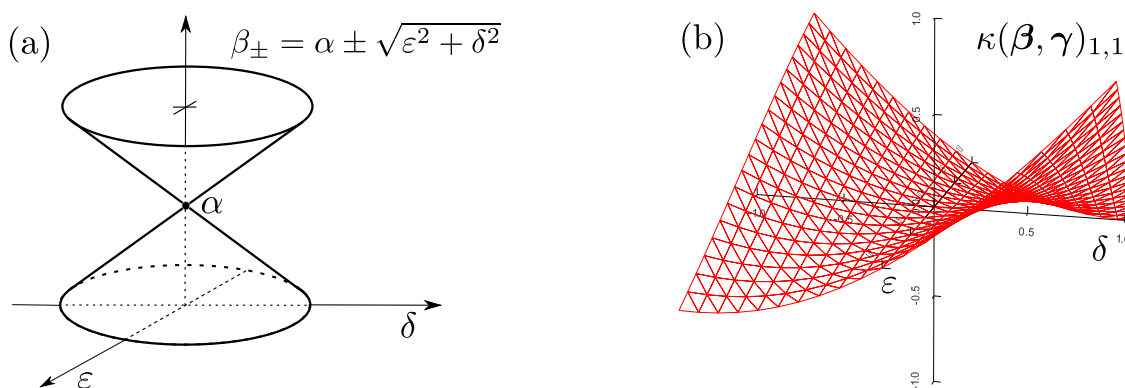


Figure 10: (a) The eigenvalue function  $\beta_{\pm} = \alpha \pm \sqrt{\varepsilon^2 + \delta^2}$ ; (b) The  $\kappa(\beta, \gamma)_{1,1}$  function, with  $\gamma = ((1, 2), (2, 3))$ .

Nevertheless, the situation is not hopeless for the  $\kappa$  function: Fig. 10.b plots the  $\kappa(\beta, \gamma)_{1,1}$  component as a function of  $(\varepsilon, \delta)$  for a specific  $\gamma$  value. Other components or  $\gamma$  values show a similar behavior. This observation suggests that  $\kappa$  is differentiable at  $(\varepsilon, \delta) = (0, 0)$  and that its derivative

is zero. Let us prove this conjecture. A careful eye of the definition (6a)-(6c) of the  $\kappa$  function shows that  $\tilde{\kappa}$  depends only upon  $(\beta_+ - \beta_-)/2 = \sqrt{\varepsilon^2 + \delta^2}$  and is independent of  $\alpha$ . More precisely, from (6b) we have  $\tilde{\kappa}_{1,2} = \hat{\kappa}(\sqrt{\varepsilon^2 + \delta^2}) \tilde{\gamma}_{1,2}$  where with  $\hat{\kappa}(x) = 1 - x/\tanh(x)$ . Then

$$\frac{\partial \tilde{\kappa}_{1,2}}{\partial \varepsilon} = \varepsilon g\left(\sqrt{\varepsilon^2 + \delta^2}\right) \tilde{\gamma}_{1,2} + \hat{\kappa}\left(\sqrt{\varepsilon^2 + \delta^2}\right) \frac{\partial \tilde{\gamma}_{1,2}}{\partial \varepsilon} \quad (17)$$

with  $g(x) = \hat{\kappa}'(x)/x$ . Observe that  $\lim_{x \rightarrow 0} g(x) = -2/3$ . Let us fix the direction  $c = \delta/\varepsilon$  and do  $\varepsilon \rightarrow 0$ . By this way  $\mathbf{v}_{\pm}$  depend only upon  $c$  and so is the unitary matrix  $\mathbf{q}$  whose columns are the normalized eigenvectors  $\mathbf{v}_{\pm}/|\mathbf{v}_{\pm}|$ . Thus  $\tilde{\gamma} = \mathbf{q}^T \boldsymbol{\gamma} \mathbf{q}$  is independent upon  $\varepsilon$ . Then, the first term of the right-hand side of (17) behaves as  $\mathcal{O}(\varepsilon)$ . We now turn to the second term of the right-hand side of (17): From one hand, we have  $\hat{\kappa}(x) = -x^2/3 + \mathcal{O}(x^3)$  and then  $\hat{\kappa}(\sqrt{\varepsilon^2 + \delta^2}) = \mathcal{O}(\varepsilon^2)$ . From other hand,  $\frac{\partial \mathbf{v}_{\pm}}{\partial \varepsilon} = \mathcal{O}(\delta^{-1}) = \mathcal{O}(\varepsilon^{-1})$  and so are  $\frac{\partial \mathbf{q}}{\partial \varepsilon}$  and  $\frac{\partial \tilde{\gamma}_{1,2}}{\partial \varepsilon}$ . Then, the second term of the right-hand side of (17) also behaves as  $\mathcal{O}(\varepsilon)$ . Finally,  $\tilde{\kappa}_{1,2}$  is differentiable in  $(0,0)$  and its derivative is zero. Now, let us turn to  $\kappa = \mathbf{q} \tilde{\kappa} \mathbf{q}^T$ . We have:

$$\frac{\partial \kappa}{\partial \varepsilon} = \frac{\partial \mathbf{q}}{\partial \varepsilon} \tilde{\kappa} \mathbf{q}^T + \mathbf{q} \frac{\partial \tilde{\kappa}}{\partial \varepsilon} \mathbf{q}^T + \mathbf{q} \tilde{\kappa} \frac{\partial \mathbf{q}^T}{\partial \varepsilon}$$

Recall that  $\mathbf{q}$  depends only upon the constant direction  $c$ . Each term behaves as  $\mathcal{O}(\varepsilon)$  and finally  $\frac{\partial \kappa}{\partial \varepsilon} = 0$  at  $(0,0)$ . As  $\varepsilon$  and  $\delta$  are interchangeable in the expression of  $\kappa$ , a similar deduction leads to  $\frac{\partial \kappa}{\partial \delta} = 0$ . Remark that, since the derivative is zero, it do not depends upon the direction  $c$ . In conclusion,  $\kappa$  is fully differentiable with respect to  $\boldsymbol{\beta}$ , even when  $\boldsymbol{\beta}$  admits multiple eigenvalues.

The `maxima` code for computing  $\kappa(\boldsymbol{\beta}, \boldsymbol{\gamma})$  writes:

```

beta : matrix([a,b],[b,c]);
gamma : matrix([g00,g01],[g10,g11]);
eig : eigenvectors(beta);
beta1 : eig[1][1][1];
beta2 : eig[1][1][2];
do_unitary(v) := v/sqrt(v[1]**2 + v[2]**2);
v1 : do_unitary(eig[2][1][1]);
v2 : do_unitary(eig[2][2][1]);
q : matrix([v1[1],v2[1]],[v1[2],v2[2]]);
tilde_gamma : transpose(q).gamma.q;
hat_kappa(x) := 1 - x/tanh(x);
k12 : hat_kappa((beta1-beta2)/2)*tilde_gamma[1][2];
tilde_kappa : matrix([0, k12],[k12,0]);
kappa : q.tilde_kappa.transpose(q);

```

The derivatives of this expression with respect to the matrix coefficients are then treated without any difficulty. As shown in this section, there are two different degeneracy cases, either when  $a = c$  or  $b = 0$ . These and these special cases are decided up to the machine precision and are treated separately. Finally, the expressions produced by `maxima` are simplified, optimized and formatted in `fortran`, `C` or `C++` for a direct use by the Euler-Newton continuation algorithm.